Article

Cell Reports

Thyroid-Hormone-Induced Browning of White Adipose Tissue Does Not Contribute to Thermogenesis and Glucose Consumption

Graphical Abstract

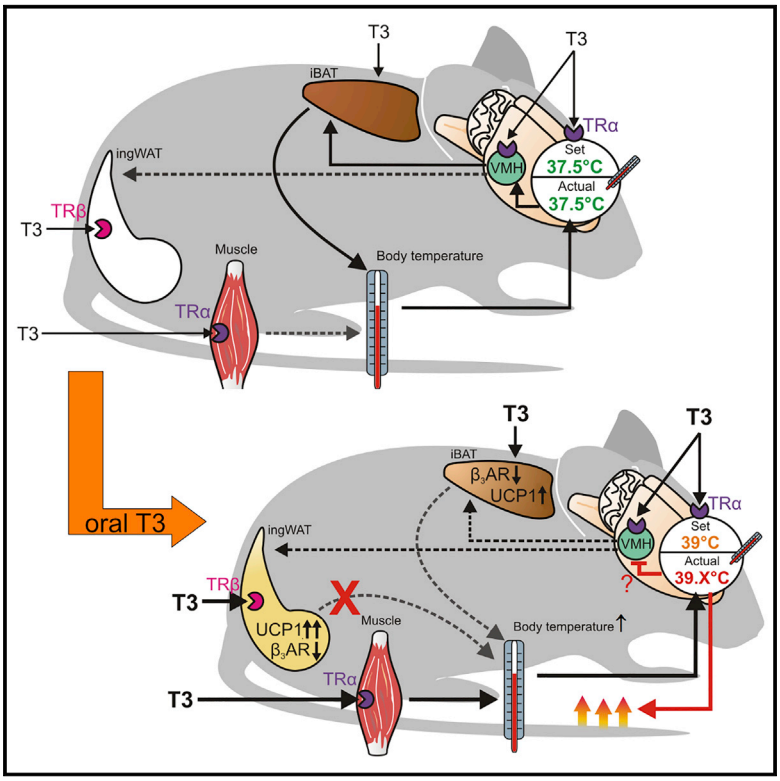

Highlights

- Thyroid hormone induces browning independent of sympathetic nervous system through TRβ
- Despite high UCP1, the beige fat lacks adrenergic input and is inactive
- Thyroid hormone's metabolic and thermogenic effects are maintained in UCP1 knockout mice
- Thyroid hormone induces hyperthermia and elevates the body temperature setpoint

Authors

Kornelia Johann, Anna Lena Cremer, Alexander W. Fischer, ..., Jeffrey W. Dalley, Heiko Backes, Jens Mittag

Correspondence

jens.mittag@uni-luebeck.de

In Brief

Thyroid hormone induces browning of white fat, but it is unclear whether this contributes to thermogenesis. Here, Johann et al. show that thyroid-hormone-induced beige fat is metabolically inactive due to lack of central stimulation and that the metabolic and thermogenic effects of the hormone are independent of UCP1.

Johann et al., 2019, Cell Reports 27, 3385–3400
June 11, 2019
https://doi.org/10.1016/j.celrep.2019.05.054

CellPress

Cell Reports
Article

Thyroid-Hormone-Induced Browning of White Adipose Tissue Does Not Contribute to Thermogenesis and Glucose Consumption

Kornelia Johann,[1] Anna Lena Cremer,[2] Alexander W. Fischer,[3] Markus Heine,[3] Eva Rial Pensado,[4,5] Julia Resch,[1] Sebastian Nock,[1] Samuel Virtue,[6] Lisbeth Harder,[1] Rebecca Oelkrug,[1] Mariana Astiz,[7] Georg Brabant,[1] Amy Warner,[6] Antonio Vidal-Puig,[6] Henrik Oster,[7] Anita Boelen,[8] Miguel López,[4,5] Joerg Heeren,[3] Jeffrey W. Dalley,[9,10] Heiko Backes,[2] and Jens Mittag[1,11,*]

[1]Internal Medicine I, Molecular Endocrinology, Center of Brain, Behavior and Metabolism, University of Lübeck, 23562 Lübeck, Germany
[2]Multimodal Imaging of Brain Metabolism, Max Planck Institute of Metabolism Research, 50931 Cologne, Germany
[3]Department of Biochemistry and Molecular Cell Biology, University Medical Center Hamburg-Eppendorf, 20246 Hamburg, Germany
[4]NeurObesity Group, Department of Physiology, CIMUS, University of Santiago de Compostela-Instituto de Investigación Sanitaria, Santiago de Compostela 15782, Spain
[5]CIBER Fisiopatología de la Obesidad y Nutrición (CIBERobn), Santiago de Compostela 15782, Spain
[6]University of Cambridge Metabolic Research Laboratories, Wellcome Trust-MRC Institute of Metabolic Science, Cambridge CB2 0QQ, UK
[7]Institute of Neurobiology, Center of Brain, Behavior and Metabolism, University of Lübeck, 23562 Lübeck, Germany
[8]Laboratory of Endocrinology, Amsterdam University Medical Centers, 1105 Amsterdam, the Netherlands
[9]Department of Psychology, University of Cambridge, Cambridge CB2 3EB, UK
[10]Department of Psychiatry, University of Cambridge, Cambridge CB2 2QQ, UK
[11]Lead Contact
*Correspondence: jens.mittag@uni-luebeck.de
https://doi.org/10.1016/j.celrep.2019.05.054

SUMMARY

Regulation of body temperature critically depends on thyroid hormone (TH). Recent studies revealed that TH induces browning of white adipose tissue, possibly contributing to the observed hyperthermia in hyperthyroid patients and potentially providing metabolic benefits. Here, we show that browning by TH requires TH-receptor β and occurs independently of the sympathetic nervous system. The beige fat, however, lacks sufficient adrenergic stimulation and is not metabolically activated despite high levels of uncoupling protein 1 (UCP1). Studies at different environmental temperatures reveal that TH instead causes hyperthermia by actions in skeletal muscle combined with a central body temperature set-point elevation. Consequently, the metabolic and thermogenic effects of systemic hyperthyroidism were maintained in UCP1 knockout mice, demonstrating that neither beige nor brown fat contributes to the TH-induced hyperthermia and elevated glucose consumption, and underlining that the mere presence of UCP1 is insufficient to draw conclusions on the therapeutic potential of browning agents.

INTRODUCTION

Obligatory thermogenesis is defined as heat resulting from maintenance of vital functions. In homeothermic species living in thermoneutral conditions, this type of thermogenesis is sufficient to maintain body temperature. Whenever the ambient temperature is reduced, heat-saving mechanisms, such as vasoconstriction, decreased movement, and piloerection, are activated, and adaptive (or facultative) thermogenesis is induced. Among these adaptive thermogenic mechanisms is the activation of non-shivering thermogenesis in brown adipose tissue (BAT). BAT thermogenesis relies on the expression of uncoupling protein 1 (UCP1) that dissociates mitochondrial substrate oxidation from ATP synthesis by introducing a proton leak, resulting in heat release (Cannon and Nedergaard, 2004). BAT is activated by the sympathetic nervous system (SNS) releasing norepinephrine (NE) that binds to β3-adrenergic receptors (ADRB3) on brown adipocytes, leading to an increase in intracellular cyclic AMP (cAMP) (Zhao et al., 1994). This rise in cAMP activates, for instance, the conversion of the thyroid hormone thyroxine (T4) to the more biologically active form 3,3′,5-triiodothyronine (T3) by the enzyme deiodinase type 2 (DIO2) (Silva and Larsen, 1983). T3 in turn increases *Ucp1* expression (Rabelo et al., 1996). BAT thermogenesis has been shown to have numerous metabolic benefits, like increased glucose and lipid uptake (Bartelt et al., 2011; Berbée et al., 2015; Greco-Perotto et al., 1987; Shibata et al., 1989; Heine et al., 2018), anti-diabetic effects, and amelioration of obesity (Bartelt et al., 2018; Kajimura et al., 2015; Svensson et al., 2016). Additionally, it was found that sustained cold exposure or certain compounds can induce brown adipocyte-like (brite or beige) cells in subcutaneous white adipose tissue of mice, a process called browning (Bartelt and Heeren, 2014; Ishibashi and Seale, 2010; Petrovic et al., 2010; Young et al., 1984). It is currently assumed that this beige fat might contribute to thermogenesis and may have beneficial metabolic effects, although the majority of studies have failed to demonstrate whether increased UCP1 in beige fat also results in higher thermogenesis or metabolism on the systemic level (Bartelt and Heeren,

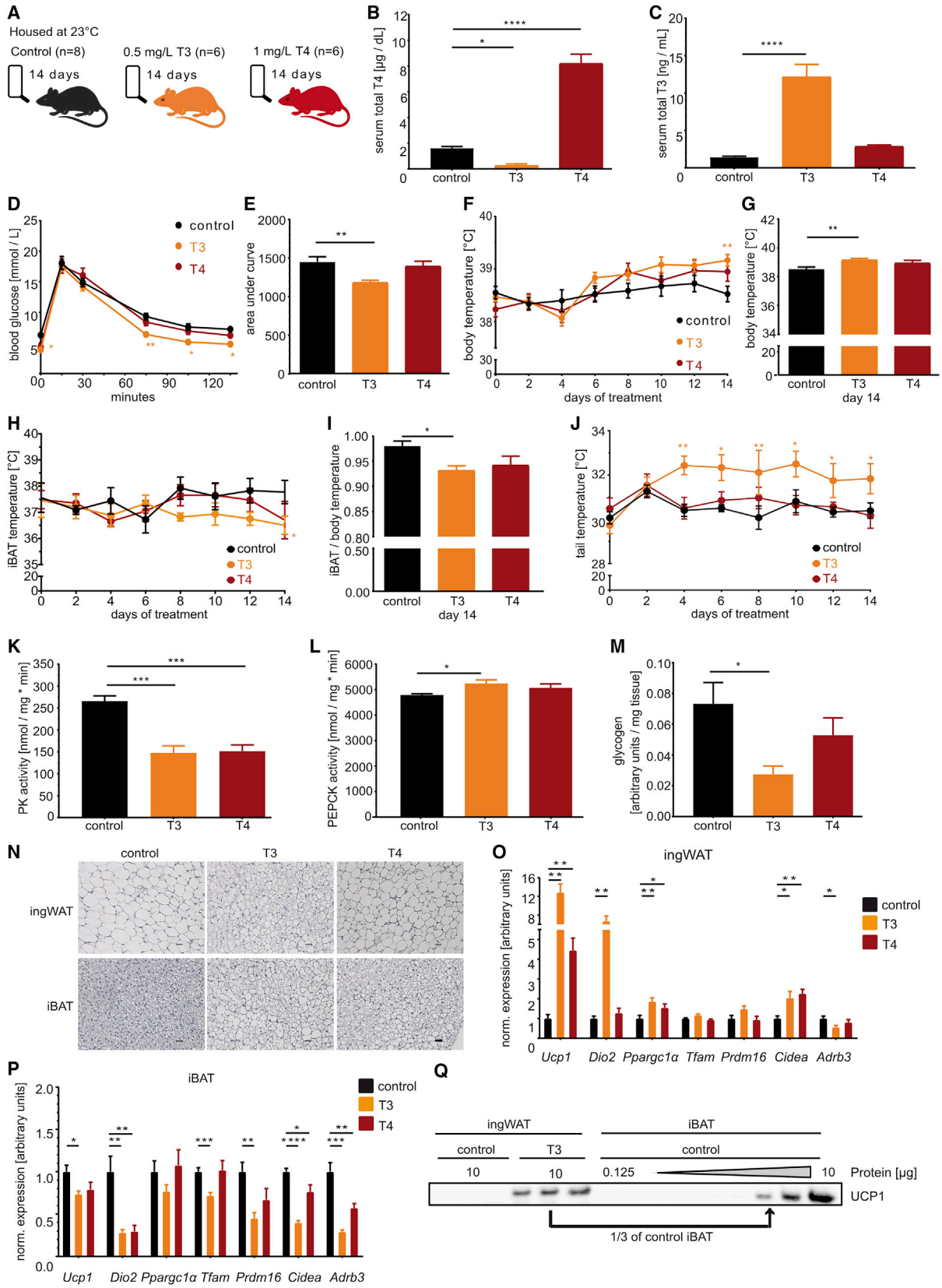

(legend on next page)

2014; Harms and Seale, 2013; Kajimura et al., 2015; Keipert and Jastroch, 2014; Warner and Mittag, 2016).

Thyroid hormones are essential in the regulation of metabolic and thermoregulatory pathways in mammals (Mullur et al., 2014; Silva, 2006; Yen, 2001). This becomes evident in hyperthyroid patients, which show impaired heat tolerance and increased body temperature (Silva, 2003). The effects of thyroid hormone on thermogenesis have been studied for decades, establishing the paradigm that the hormone increases obligatory thermogenesis in several tissues, including muscle, which leads to a higher body temperature (Silva, 2006). Thyroid hormones exert their actions by the nuclear thyroid hormone receptors (TRs) alpha1 (TRα1), beta1 (TRβ1), or beta 2 (TRβ2), altering gene expression (Sap et al., 1986; Tata, 1986; Thompson et al., 1987). TRs are expressed in almost every tissue and often have overlapping functions; however, there are tissues that predominantly rely on TRα1 or TRβ, respectively (Yen, 2001). With regard to thermogenesis, TRβ has been shown to play a role in the regulation of adaptive thermogenesis by regulating *Ucp1* mRNA expression, and TRα1 seems to modulate adrenergic sensitivity (Ribeiro et al., 2001; Weiss et al., 1998). However, mice devoid of all TRs still display competent BAT recruitment and *Ucp1* gene expression but depressed thermogenesis, suggesting a complex interplay between thyroid hormone and body temperature regulation (Golozoubova et al., 2004). Moreover, it was recently discovered that TRα1 also controls tail heat loss with secondary effects for BAT thermogenesis (Warner et al., 2013). Therefore, thyroid hormones are relevant for almost all aspects of thermoregulation, including thermal conductance as well as obligatory and facultative thermogenesis. In addition to the peripheral actions, recent studies revealed that thyroid hormone also induces facultative thermogenesis through central mechanisms, as central hyperthyroidism leads to direct activation of BAT in an AMP-activated protein kinase (AMPK)-dependent manner in rats (Alvarez-Crespo et al., 2016; López et al., 2010; Martínez-Sánchez et al., 2017b) and induces browning in mice (Martínez-Sánchez et al., 2017a). Most interestingly, a recent study revealed that the TRβ agonist GC-1 directly triggers browning (Lin et al., 2015), an effect that has been reported for thyroid hormone as well (Hoefig et al., 2016; Weiner et al., 2016). The data suggested that the beige fat recruitment could contribute to the body temperature increase observed in hyperthyroidism and might provide favorable metabolic effects. The findings therefore challenge the well-established model that thyroid hormone only modulates basal metabolic rate and obligatory thermogenesis (Silva, 2006) and indicate that beige fat might be a prominent player in the thermogenic and metabolic effects of the hormone. Therefore, we aimed to test the role of thermogenic adipose tissue in body temperature regulation and for the metabolic benefits observed in systemic hyperthyroidism.

RESULTS

Hyperthyroidism Improves Glucose Tolerance and Induces Browning of Inguinal White Adipose Tissue

To establish the effects of hyperthyroidism, wild-type (WT) mice were treated for 14 days with either 0.5 mg/L T3 or 1 mg/L T4 in drinking water (Figure 1A). Treatment with T3 induced a substantial hyperthyroidism with an 8.5-fold increase in serum total T3 (tT3) and a 90% decrease in serum tT4 (Figures 1B and 1C). Hyperthyroidism was fully achieved after 24 h (not shown), persistently observed over the course of a day (Figures S1A and S1B), and leads to a complete suppression of pituitary thyroid-stimulating hormone (TSH) (Figure S1C). It was accompanied by an increase in energy expenditure, a lower respiratory quotient, and an increase in body weight and length as expected (Neilsen, 1953; Rakov et al., 2016; Green, 1975), as well as hyperphagia (Figures S1D–S1H). Our model for T4-induced hyperthyroidism was milder, with no significant elevation in tT3 and a 7.4-fold increase in serum tT4 (Figures 1B and 1C) but no significant changes in body weight, length, or food intake (Figures S1F–S1H). As hyperthyroidism is associated with improved glucose tolerance, we performed an intraperitoneal glucose tolerance test (ipGTT) and found reduced blood glucose levels in T3-treated, but not T4-treated, mice (Figures 1D and 1E; $p < 0.01$ for T3; $p = 0.34$ for T4; repeated measures [RM]-ANOVA). Core body temperature in thyroid-hormone-treated mice started to increase after 1 week of treatment (Figure 1F) and was significantly elevated in T3-treated, but not T4-treated, mice after 2 weeks (T3 $p < 0.01$; T4 $p = 0.09$; Figure 1G). Skin temperature above the interscapular brown adipose tissue (iBAT) as measured by infrared thermography did not significantly change

Figure 1. Hyperthyroidism Improves Glucose Tolerance and Induces Browning of ingWAT

(A) Scheme of treatment regimen for induction of hyperthyroidism in mice.
(B) Serum total T4 levels after 14 days of treatment.
(C) Serum total T3 levels after 14 days of treatment.
(D) ipGTT after 12 days of treatment with THs.
(E) Area under curve (AUC) of ipGTT (D).
(F) Rectal temperature of control and T3- and T4-treated mice over 14 days of treatment.
(G) Rectal temperature at the end of treatment.
(H) iBAT temperature as measured by infrared thermography over 14 days of treatment.
(I) iBAT temperature as measured by infrared thermography at the end of treatment normalized to rectal temperature.
(J) Tail temperature of control and T3- and T4-treated mice as measured by infrared thermography over 14 days of treatment.
(K) Hepatic PK activity in control and T3- and T4-treated mice.
(L) Hepatic PEPCK activity in control and T3- and T4-treated mice.
(M) Hepatic glycogen content of control and T3- and T4-treated mice.
(N) Representative H&E stainings of iBAT and ingWAT of control and T3- and T4-treated mice. Scale bar 10 μm.
(O and P) Gene expression analysis in (O) ingWAT and (P) iBAT in control and T3- and T4-treated mice.
(Q) Direct comparison of ingWAT UCP1 protein expression of T3-treated mice to control iBAT.
Data are presented as mean ± SEM; n = 6–8. *$p < 0.05$; **$p < 0.01$; ***$p < 0.001$. See also Figure S1.

over the course of the 14 days of treatment (Figures 1H and S1I) but was significantly decreased upon T3 at the end of the treatment, in absolute values but also when normalized to body temperature (Figures 1H and 1I). In parallel, skin temperature above the inguinal white adipose tissue (ingWAT) was unchanged (Figure S1J). Interestingly, tail temperature was significantly elevated over the course of the T3 treatment indicative of vasodilation to dissipate excess heat starting at day 4 of the treatment (Figure 1J). To further investigate glucose metabolism, we measured the activities of rate-limiting steps in glycolysis (pyruvate kinase [PK]) and gluconeogenesis (phosphoenolpyruvate-carboxykinase [PEPCK]) in liver. PK activity was significantly decreased in T3- and T4-treated mice (Figure 1K), and PEPCK activity was increased in T3-treated mice (Figure 1L). Hepatic glycogen content was decreased in T3-treated mice (Figure 1M), indicating a higher systemic need for glucose. Organ weights determined at the time of sacrifice showed the expected cardiac hypertrophy in T3-treated, but not T4-treated, mice (Figures S1K and S1L). In both T3- and T4-treated animals, iBAT depots were significantly larger and appeared paler, suggesting higher lipid deposition (Figure S1M), which was confirmed by H&E staining (Figure 1N). Interestingly, when we investigated ingWAT morphology (Figure 1N), an increase in smaller, multilocular fat cells was observed, indicating induction of browning by thyroid hormone, as reported previously (Alvarez-Crespo et al., 2016; Finan et al., 2016; Weiner et al., 2016). To test this on the molecular level, we measured gene expression of thermogenic marker genes (*uncoupling protein 1* [*Ucp1*]; *deiodinase 2* [*Dio2*]; *peroxisome proliferator-activated receptor gamma coactivator 1 alpha* [*Ppargc1α*]; *mitochondrial transcription factor A* [*Tfam*]; *PR domain containing 16* [*Prdm16*]; *cell-death-inducing DFFA-like effector a* [*Cidea*]; *β3-adrenergic receptor* [*Adrb3*]; Figures 1O and 1P) and UCP1 protein expression (Figure 1Q). In ingWAT, we found an elevation of several thermogenic markers, including *Ucp1*, *Dio2*, *Ppargc1α*, and *Cidea* in T3- and T4-treated animals, and *Adrb3* mRNA was reduced upon T3 treatment (Figure 1O). In contrast, iBAT gene expression analysis showed a decrease in most thermogenic and brown fat marker genes (Figure 1P). Interestingly, despite reduced mRNA levels, UCP1 protein was elevated in T3-treated iBAT with no change in the protein level of the mitochondrial respiratory chain complexes (Figures S1N–S1P). In T3-treated ingWAT, UCP1 protein reached levels comparable to about one-third of the amount found in untreated iBAT (Figure 1Q), suggesting a possibly high thermogenic potential. Browning was also induced by T3 and T4 in gonadal WAT (gWAT) on the mRNA level (Figure S1Q); however, no significant amount of UCP1 protein was detectable in this tissue (Figure S1R). Given that the T3 treatment entirely suppressed TSH, thus potentially blocking the oscillating rhythm of thyroid hormone secretion, we tested whether the lack of a circadian rhythm would by itself cause browning. Using clock-deficient *Per1/Per2* double mutant (double knockout [DKO]) mice, we confirmed that this was not the case, as *Ucp1* mRNA expression was not induced in ingWAT (Figure S1S). Taken together, these data show that T3 and T4 are capable of browning ingWAT on the molecular level; however, the systemic effects of hyperthyroidism are more pronounced in the T3-treated group.

Ucp1 Expression in ingWAT Is Dependent on TRβ

As it was reported that browning of ingWAT can be induced by TRβ-selective compounds (Lin et al., 2015), we investigated the metabolic phenotype of global TRβ knockout (KO) mice (Figure 2A). These mice showed elevated serum tT3 and tT4 levels (Figures S2A and S2B) due to the impaired feedback of the hypothalamus-pituitary-thyroid axis (Forrest et al., 1996). Although ipGTT was not altered in TRβ KO mice compared to their WT littermates (Figures 2B and 2C; $p = 0.41$ for TRβ; RM-ANOVA), their basal metabolic rate (BMR) (defined here as metabolism at thermoneutrality) was significantly increased (Figures 2D and 2E). This did, however, not translate to an increase in daily energy expenditure at room temperature (Figures S2C and S2D), suggesting a compensatory adaptation of non-shivering thermogenesis. Despite being hyperthyroid, TRβ KO mice did not have elevated body or iBAT temperature (Figures 2F–2H), and the histology of iBAT and ingWAT was similar to controls (Figure 2I). When investigating gene expression in ingWAT, we found that *Dio2* and *Adrb3* expression were not altered in hyperthyroid TRβ KO mice, but *Ucp1* mRNA expression was even lower than in controls (Figure 2J). In iBAT, *Ucp1* expression was not altered on mRNA (Figure 2K) or protein level (Figures S2E and S2F). These data demonstrate that browning of ingWAT by thyroid hormone on the molecular level depends on intact TRβ signaling.

Hyperthyroidism Decreases Adipose Tissue Glucose and Lipid Uptake

Activation of thermogenesis in adipose tissues is associated with increased glucose uptake (Cannon and Nedergaard, 2004). To test this directly, we performed [18]fluoro-2-deoxyglucose–positron emission tomography (^{18}FDG-PET)/computed tomography (CT) scans of T3- and T4-treated mice. Despite elevated UCP1 levels, ingWAT glucose uptake was not increased but decreased upon systemic T3 or T4 treatment (Figures 3A and 3B). Likewise, glucose uptake in iBAT was reduced (Figures 3C and 3D), and no change was observed in gWAT or soleus muscle (Figures S2G and S2H). ^{18}FDG-PET/CT may, however, not accurately reflect brown or beige fat thermogenic activity (Hankir et al., 2017; Olsen et al., 2017), as thermogenesis is mainly fueled by fatty acids (Bartelt et al., 2011; Cannon and Nedergaard, 2004). We therefore also measured uptake of triglyceride-rich lipoproteins (TRLs) in hyperthyroid mice. In iBAT, TRL uptake significantly decreased to about one-third in systemically T3- and T4-treated mice, and no difference was observed in ingWAT (Figure 3E). Given the lack of metabolic activation in the presence of elevated UCP1 protein levels, we hypothesized that the thermogenic capacity of the tissue might not be fully exploited due to insufficient adrenergic stimulation. Therefore, we injected mice with 1 mg/kg NE to stimulate maximum non-shivering thermogenesis. Control and T3-treated animals showed an elevation in oxygen consumption after NE injection (Figure 3F); however, the response was more pronounced in T3-treated mice, indicating a higher thermogenic capacity. Our hypothesis of insufficient adrenergic stimulation was further supported on the molecular level, as we found no significant elevation in ingWAT and iBAT of intracellular cAMP (Figures 3G and 3H), phosphohormone sensitive lipase (HSL; Figures 3I and 3J), or free fatty acids (Figures 3K and 3L), which are required for activation of

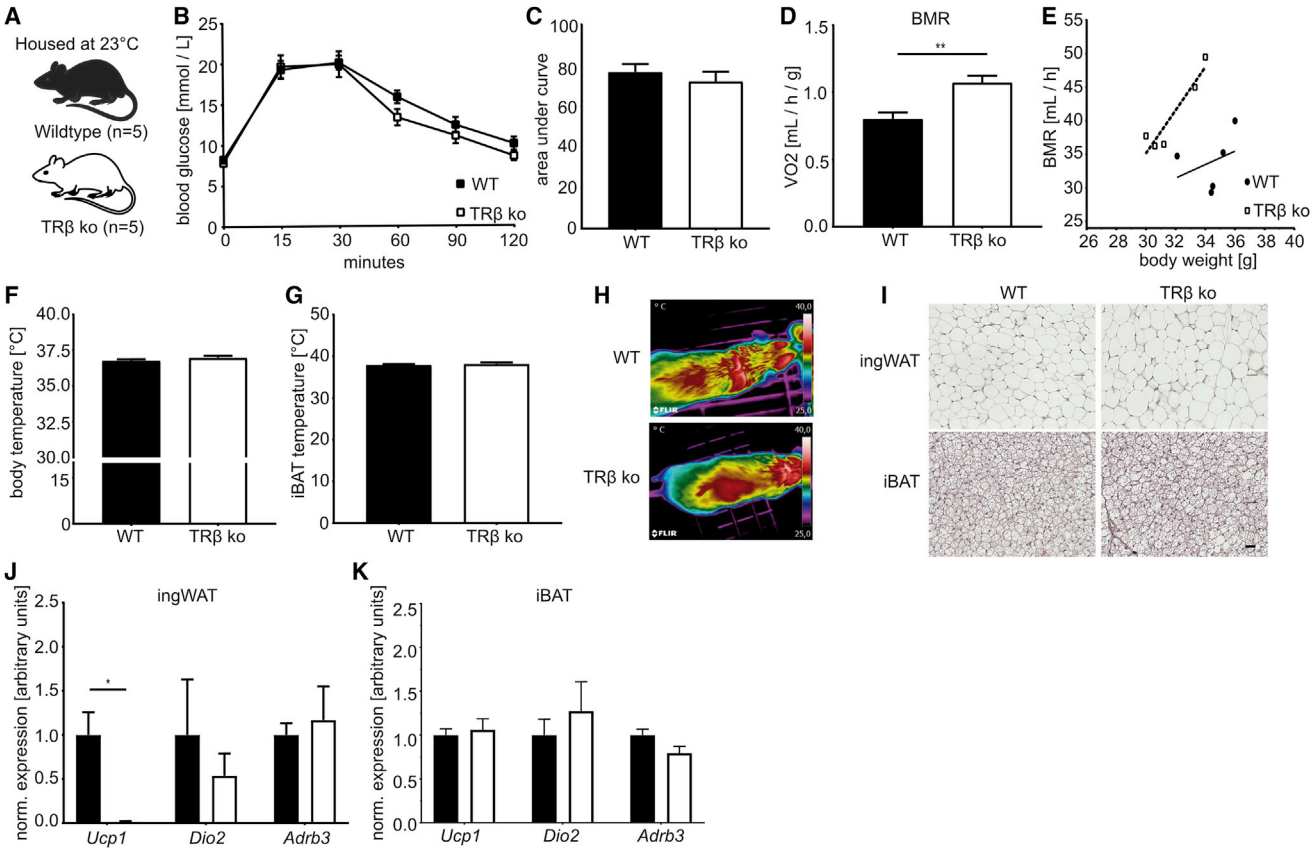

Figure 2. *Ucp1* Expression in ingWAT Is Dependent on TRβ Expression

(A) Adult TRβ KO mice and their WT littermates were metabolically characterized.
(B) ipGTT of WT and TRβ KO mice.
(C) Area under curve of ipGTT (B).
(D) BMR of WT and TRβ KO mice normalized to body weight.
(E) BMR of WT and TRβ KO mice plotted against body weight.
(F) Rectal temperature of WT and TRβ KO mice.
(G) iBAT temperature as measured by infrared thermography.
(H) Representative infrared pictures of iBAT of WT and TRβ KO mice.
(I) Representative H&E stainings of ingWAT and iBAT of WT and TRβ KO mice. Scale bar 10 μm.
(J and K) Gene expression analysis of (J) ingWAT and (K) iBAT of WT and TRβ KO mice.
Data are presented as mean ± SEM; n = 5. *p < 0.05; **p < 0.01; ***p < 0.001. See also Figure S2.

UCP1 (Shabalina et al., 2010). Interestingly, expression of genes involved in lipogenesis and lipolysis (*peroxisome proliferator-activated receptor gamma* [*Pparγ*]; *fatty acid translocase* [*Cd36*]; *carbohydrate-responsive element-binding protein beta* [*Chrebpb*]; *lipoprotein lipase* [*Lpl*]; *leptin* [*Lep*]; *lipase A* [*Lipa*]; *stearoyl-coenzyme A* [*CoA*] *desaturase 1* [*Scd1*]; *fatty acid synthase* [*Fasn*]) was mostly unaltered in ingWAT (Figure S2I) while being reduced in iBAT of hyperthyroid mice (Figure S2J). Collectively, these data suggest that, despite a molecular browning fingerprint including elevated UCP1 protein, the metabolic turnover is not elevated in thermogenic adipose tissues of hyperthyroid animals.

Thyroid-Hormone-Induced Hyperthermia Is Independent of SNS Signaling in Adipose Tissues

T3 centrally activates thermogenesis via the SNS (Alvarez-Crespo et al., 2016; López et al., 2010; Martínez-Sánchez et al., 2017b). Interestingly, we observed a downregulation of *Adrb3* expression in iBAT and ingWAT in systemic hyperthyroidism, suggesting reduced adrenergic responsiveness of these tissues. We then measured NE turnover in hyperthyroid mice (Figures S3A and S3B). The data revealed that baseline NE levels (0 h) and NE turnover were not significantly different between controls and T3- or T4-treated mice at room temperature in ingWAT but lower in iBAT (Figures 4A, 4B, S3C, and S3D). This was accompanied by normal levels of tyrosine hydroxylase protein in both tissues (Figures S3E–S3G) and suggests that the elevation of body temperature in systemically hyperthyroid animals might not be caused by a central activation of the SNS. To elucidate this in greater detail, we housed mice at thermoneutrality (TN) (Figure 4C), where thermogenic adipose tissue is only minimally innervated due to the lack of facultative thermogenesis (Cannon and Nedergaard, 2004; Sjögren et al., 2007).

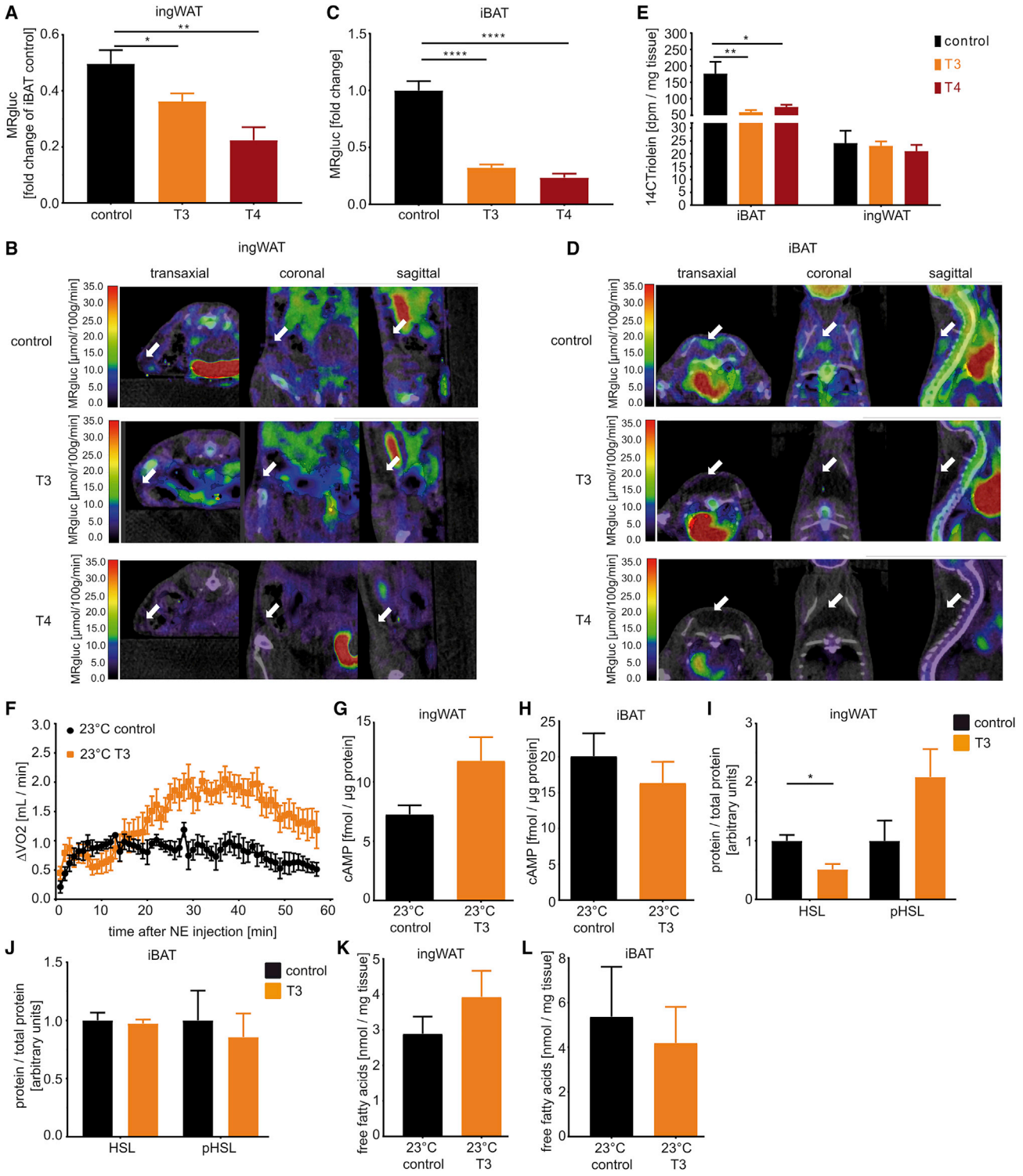

Figure 3. Hyperthyroidism Decreases Adipose Tissue Glucose and Lipid Uptake

(A) Rate of glucose metabolism in ingWAT of control and hyperthyroid mice after 14 days of treatment as measured by ^{18}FDG-PET/CT. n = 7–14.

(B) Representative ^{18}FDG-PET/CT pictures of ingWAT of control and hyperthyroid mice. White arrows indicate ingWAT depot analyzed.

(C) Rate of glucose metabolism in iBAT of control and hyperthyroid mice after 14 days of treatment as measured by ^{18}FDG-PET/CT. n = 7–14.

(D) Representative ^{18}FDG-PET/CT pictures of iBAT of control and hyperthyroid mice. White arrows indicate iBAT depot analyzed.

(E) Uptake of radioactively labeled TRLs into ingWAT and iBAT of control and T3- and T4-treated mice after 14 days of treatment. n = 7–8.

(legend continued on next page)

Interestingly, TN-housed mice still displayed a significantly elevated body temperature already after 1 day of treatment with T3 (Figures 4D, 4E, S3H, and S3I). As expected, NE levels in ingWAT (Figures 4F and S3J) as well as iBAT (Figures 4G and S3K) were strongly reduced at TN as compared to room temperature. Only when normalized to tissue weight, but not protein content, T3 caused a significantly further decline of NE in iBAT at both temperatures (Figures 4G and S3K). In both tissues, no significant change was observed in intracellular cAMP (Figures 4H and 4I) and free fatty acids (Figures 4J and 4K). Interestingly, ingWAT of T3-treated mice at TN still showed histological signs of browning (Figure 4L), together with increased expression of *Ucp1*, albeit at much lower levels (Figure 4M; Table S1). As expected, we found "whitened iBAT" in control and T3-treated mice at TN characterized by bigger, unilocular cells (Figure 4L). The lower *Ucp1* gene expression in iBAT by systemic T3 treatment was reversed at TN (Figure 4N; Table S1), which together with elevated UCP1 protein (Figure 4O) suggests a "re-browning" of the whitened iBAT by T3. Together, our data implicate that the increase in body temperature and the browning of ingWAT in systemic hyperthyroidism occur independently of SNS activation. Moreover, the beige fat seems to lack thermogenic activity due to insufficient sympathetic stimulation. Interestingly, this is opposite to what is observed in central hyperthyroidism, which is characterized by marked SNS activation (López et al., 2010; Martínez-Sánchez et al., 2017b). We therefore tested whether the AMPK pathway in the ventromedial nucleus of the hypothalamus (VMH) is triggered by the systemic T3 treatment. Our data revealed that there was no effect of the systemic T3 treatment at 23°C or 30°C on AMPKα phosphorylation in the VMH (Figures 4P–4S), despite T3 reaching the brain as evidenced by the T3-induced hypothalamic genes *Dio3*, *Hr*, and *Klf9* (Figure S3L), as well as significantly increased hypothalamic T3 content (Figure S3M).

Thyroid-Hormone-Mediated Increase in Body Temperature Persists in the Cold

To test whether alleviating the heat stress of the T3 treatment normalizes body temperature regulation, we repeated the treatment at 10°C (Figures 5A, S3N, and S3O). Interestingly, the elevation of body temperature by T3 persisted in these animals (Figure 5B) with normal iBAT (Figures 5C and 5D) and tail temperature (Figure 5E), indicating the absence of hyperthermia and a centrally elevated body temperature setpoint. Interestingly, T3 still induced browning of ingWAT at the histological level, and iBAT contained more fat droplets, comparable to the situation at higher temperatures (Figure 5F). However, on the molecular level (Figures 5G and S3P), *Ucp1* mRNA was not significantly higher in the T3-treated group, most likely because the ingWAT of control animals was browned by the lower temperature. Only *Dio2* mRNA levels were still elevated by the T3 treatment (Figure 5G). In contrast, iBAT showed lower expression of thermogenic genes and *Adrb3* in the T3 group (Figures 5H and S3Q), with normal UCP1 protein (Figure 5I). The NE stimulation test showed a stronger response in both groups and a smaller difference between T3-treated and untreated animals (Figure 5J), suggesting a lower additional effect of T3 on thermogenic capacity at 10°C as compared to 23°C. We observed comparable levels of NE and intracellular cAMP in ingWAT and iBAT of both groups (Figures 5K–5N, S3R, and S3S). Interestingly, free fatty acids were significantly elevated in ingWAT of T3-treated mice, and no difference was found in iBAT (Figures 5O and 5P). When we analyzed the VMH, we observed that now, in the absence of heat stress as evidenced by the normal tail temperature, AMPKα phosphorylation was reduced by the T3 treatment (Figures 5Q and 5R).

Thyroid-Hormone-Mediated Increase in Body Temperature Is Independent of UCP1

As neither beige nor brown fat appeared to be active in hyperthyroid mice at room temperature, we hypothesized that the observed hyperthermia might not depend on UCP1-mediated thermogenesis. To test this directly, we treated UCP1 KO mice and their WT littermates at room temperature with T3 (Figure 6A), resulting in both genotypes in a decrease in serum tT4 and a strong increase in serum tT3 (Figures S4A and S4B) and reduced blood glucose levels in the ipGTT (Figures 6B and 6C; ipGTT: $p_{genotype} = 0.466$, $p_{T3} < 0.0006$, and $p_{interaction} = 0.892$). The relative amount of lean mass was increased in T3-treated WT and UCP1 KO mice, and the relative amount of fat mass was not significantly altered (Figures S4C and S4D; lean mass: $p_{genotype} = 0.721$, $p_{T3} < 0.0008$, and $p_{interaction} = 0.065$; fat mass: $p_{genotype} = 0.458$, $p_{T3} = 0.565$, and $p_{interaction} = 0.069$). Body temperature was significantly elevated in both groups after treatment with T3 (Figure 6D; body temperature: $p_{genotype} = 0.794$, $p_{T3} < 0.0001$, and $p_{interaction} = 0.213$). Interestingly, we found multilocular cells in ingWAT of UCP1 KO mice after T3 treatment as a histological sign of browning, and the multilocular cells in the iBAT of these mice appeared bigger (Figure 6E). Moreover, we found an increased expression of *Cidea* after T3 treatment in UCP1 KO mice, and most other markers of browning were not altered in ingWAT (Figure 6F; Table S2). iBAT gene expression of WT and UCP1 KO mice showed a decrease in *Adrb3*, *Dio2*, and *Ppargc1α* in systemic hyperthyroidism (Figure 6G; Table S2). It was reported that ingWAT features other thermogenic mechanisms, like calcium or creatine cycling (Ikeda et al., 2017; Kazak et al., 2015, 2017); however, we only found a minor increase in *Serca2* (*Atp2a2*) gene expression in ingWAT of T3-treated WT

(F) Change in oxygen consumption of control and T3-treated mice housed at 23°C after NE injection. n = 6.
(G) cAMP levels in ingWAT of mice housed and treated at 23°C. n = 4.
(H) cAMP levels in iBAT of mice housed and treated at 23°C. n = 4.
(I) Protein expression of HSL and phospho HSL (pHSL) in ingWAT of mice housed and treated at 23°C. n = 4.
(J) Protein expression of HSL and pHSL in iBAT of mice housed and treated at 23°C. n = 4.
(K) Free fatty acids in ingWAT of mice housed and treated at 23°C. n = 4.
(L) Free fatty acids in iBAT of mice housed and treated at 23°C. n = 4.
Data are presented as mean ± SEM. *p < 0.05; **p < 0.01; ***p < 0.001. See also Figure S2.

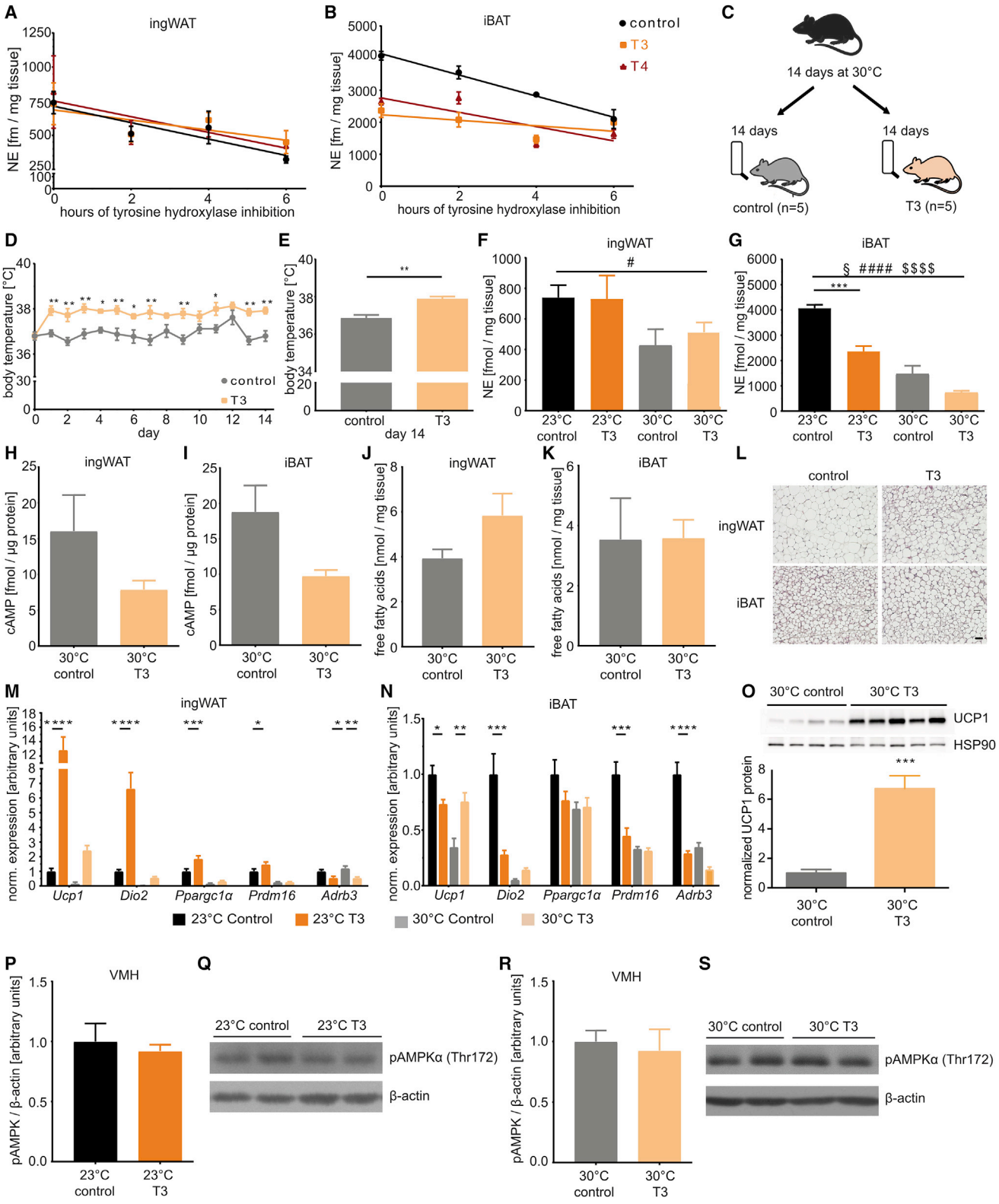

Figure 4. Thyroid-Hormone-Induced Hyperthermia Is Independent of SNS Signaling

(A and B) NE turnover in (A) ingWAT and (B) iBAT of control and T3- and T4-treated mice after 14 days of treatment normalized against tissue weight. n = 4 per time point and group.

(legend continued on next page)

and UCP1 KO mice, and markers of creatine metabolism (*glycine amidinotransferase* [*Gatm*]; *guanidinoacetate N-methyltransferase* [*Gamt*]; *mitochondrial creatine kinase 1 and 2* [*Ckmt1 and Ckmt2*]; *creatine transporter 1 or solute carrier family 6 member 8* [*Slc6a8*]; *phosphoethanolamine/phosphocholine phosphatase* [*Phospho1*]) were unchanged in ingWAT or iBAT (Figures S4E and S4F; Table S2).

Given these results, we hypothesized that the muscle as the other main thermogenic tissue could be responsible for the hyperthermia. This was supported by an elevated resting metabolic rate (fasted and measured at 30°C) in T3-treated WT mice (Figure 6H), an increased TRL uptake in M. Soleus (Figure 6I), a mainly lipolytic muscle type as evidenced by normal glucose uptake (Figure S2H). Intramuscular glycogen was decreased in M. Gastrocnemius (Figure 6J) in the presence of mildly elevated PK enzyme activity (Figure S4G), as expected from a hyperthyroid muscle (Salvatore et al., 2014). On the molecular level, this was accompanied by an alteration of several genes involved in regulating energy expenditure in both muscle types, including the uncoupling protein *Ucp3*, the mitochondrial shuttle *Gpd2*, or genes connected to calcium handling (*uncoupling protein 3* [*Ucp3*]; *glycerol-3-phosphate dehydrogenase 2* [*Gpd2*]; *peroxisome proliferator activated receptor delta* [*Pparδ*]; *sarcolipin* [*Sln*]; *ryanodine receptor 1* [*Ryr1*]; *ATPase $Na^+/K+$ transporting subunit alpha 2* [*Atp1a2*]; *glucose transporter 1* [*Slc2a1, Glut1*]; *glucose transporter 4* [*Slc2a4, Glut4*]; *lactate dehydrogenase a* [*Ldha*]; Figures 6K, 6L, S4H, and S4I). Likewise, we observed increased SERCA2 protein in M. Soleus, together with an induced expression of mitochondrial respiratory complex proteins (Figures 6M–6O). Taken together, these findings show that the metabolic effects of T3 contributing to the hyperthermia at 23°C are caused by skeletal muscle rather than thermogenic adipose tissue.

DISCUSSION

Thyroid hormones are essential components in the regulation of metabolism (López et al., 2013; Mullur et al., 2014; Silva, 2006; Warner and Mittag, 2012; Yen, 2001). Although it is well known that hyperthyroidism increases body temperature, the mechanism remains controversial. The classic paradigm states that hyperthyroidism leads to an increase in basal metabolic rate and obligatory thermogenesis, presumably through actions in skeletal muscle (Santhanam et al., 2018; Silva, 2006). This simple concept was challenged recently by studies showing that central T3 can directly activate BAT thermogenesis via hypothalamic AMPK signaling (Alvarez-Crespo et al., 2016; López et al., 2010; Martínez-Sánchez et al., 2017b) and that the hormone as well as the TRβ agonist GC-1 cause browning (Lin et al., 2015; Weiner et al., 2016). Moreover, thyroid hormones also play an important role in the regulation of heat dissipation over the tail surface (Warner et al., 2013). Together, these studies demonstrated that the regulation of body temperature by thyroid hormone might be multi-layered and more complex than previously thought. Our study now clarifies the individual contributions of these different pathways to whole body thermoregulation in systemic hyperthyroidism.

In ingWAT, we found a strong induction of browning in hyperthyroidism, with UCP1 reaching levels comparable to about one-third of those found in iBAT. This required TRβ, as browning was absent in hyperthyroid TRβ KO mice. The precise mechanism remains yet to be elucidated but could be mediated by a direct activation of the browning program in white adipose tissue, as T3 is known to directly induce the expression of *Ucp1* in iBAT (Rabelo et al., 1995; Silva, 2006) or by the induction of *Fgf21* expression in liver (not shown), which can also induce browning (Finan et al., 2016; Fisher et al., 2012; Hotta et al., 2009; Inagaki et al., 2007; Kharitonenkov et al., 2005). Further studies employing a tool to obtain a precise browning fingerprint (Cheng et al., 2018) may shed light on the underlying mechanism.

In line with the direct effect of T3 on peripheral TRβ, the browning by thyroid hormone seems to be independent of the SNS, as neither NE nor cAMP content in hyperthyroid ingWAT were elevated, and it was still observed at thermoneutrality, where adipose tissue is functionally denervated (Cannon and Nedergaard, 2004). Surprisingly, ^{18}FDG-PET/CT and TRL uptake studies demonstrated that the beige adipose tissue induced by T3 is neither metabolically nor thermogenically active and might not contribute to the hyperthermia despite high UCP1. This was further supported in iBAT by increased lipid deposition and elevated leptin expression indicative of a switch to a more white-fat-like phenotype (Frederich et al., 1995), decreased

(C) Schematic representation of housing and treatment regimen of WT mice at thermoneutrality.
(D) Rectal temperature of control and T3-treated mice over 14 days of treatment at thermoneutrality. n = 5.
(E) Rectal temperature at day 14 of treatment at thermoneutrality. n = 5.
(F and G) NE content of (F) ingWAT and (G) iBAT of control and T3-treated mice at 23°C and 30°C. n = 4–5.
(H) cAMP levels in ingWAT of mice housed and treated at 30°C. n = 5.
(I) cAMP levels in iBAT of mice housed and treated at 30°C. n = 5.
(J) Quantification of free fatty acids in ingWAT of mice housed and treated at 30°C. n = 5.
(K) Quantification of free fatty acids in iBAT of mice housed and treated at 30°C. n = 5.
(L) Representative H&E stainings of control and T3-treated ingWAT and iBAT. Mice were housed and treated at thermoneutrality. Scale bar 10 μm.
(M and N) Gene expression analysis in (M) ingWAT and (N) iBAT of control and T3-treated mice housed and treated at 23°C or 30°C, respectively. n = 5–8.
(O) UCP1 protein levels in iBAT of control and T3-treated mice housed and treated at 30°C.
(P) Quantification of pAMPKα in the VMH of mice housed and treated with T3 at 23°C. n = 4.
(Q) Representative western blot of pAMPKα expression in the ventromedial hypothalamus (VMH) of mice housed and treated with T3 at 23°C.
(R) Quantification of pAMPKα in the VMH of mice housed and treated with T3 at 30°C. n = 3–5.
(S) Representative western blot of pAMPKα expression in the VMH of mice housed and treated with T3 at 30°C.
Data are presented as mean ± SEM. *p < 0.05; **p < 0.01; ***p < 0.001; $^{\S}p_{Interaction} < 0.05$; $^{\#}p_{ambient\ temperature} < 0.05$; $^{\#\#\#\#}p_{ambient\ temperature} < 0.0001$; $^{\$\$\$\$}p_{T3} < 0.0001$. See also Figure S3.

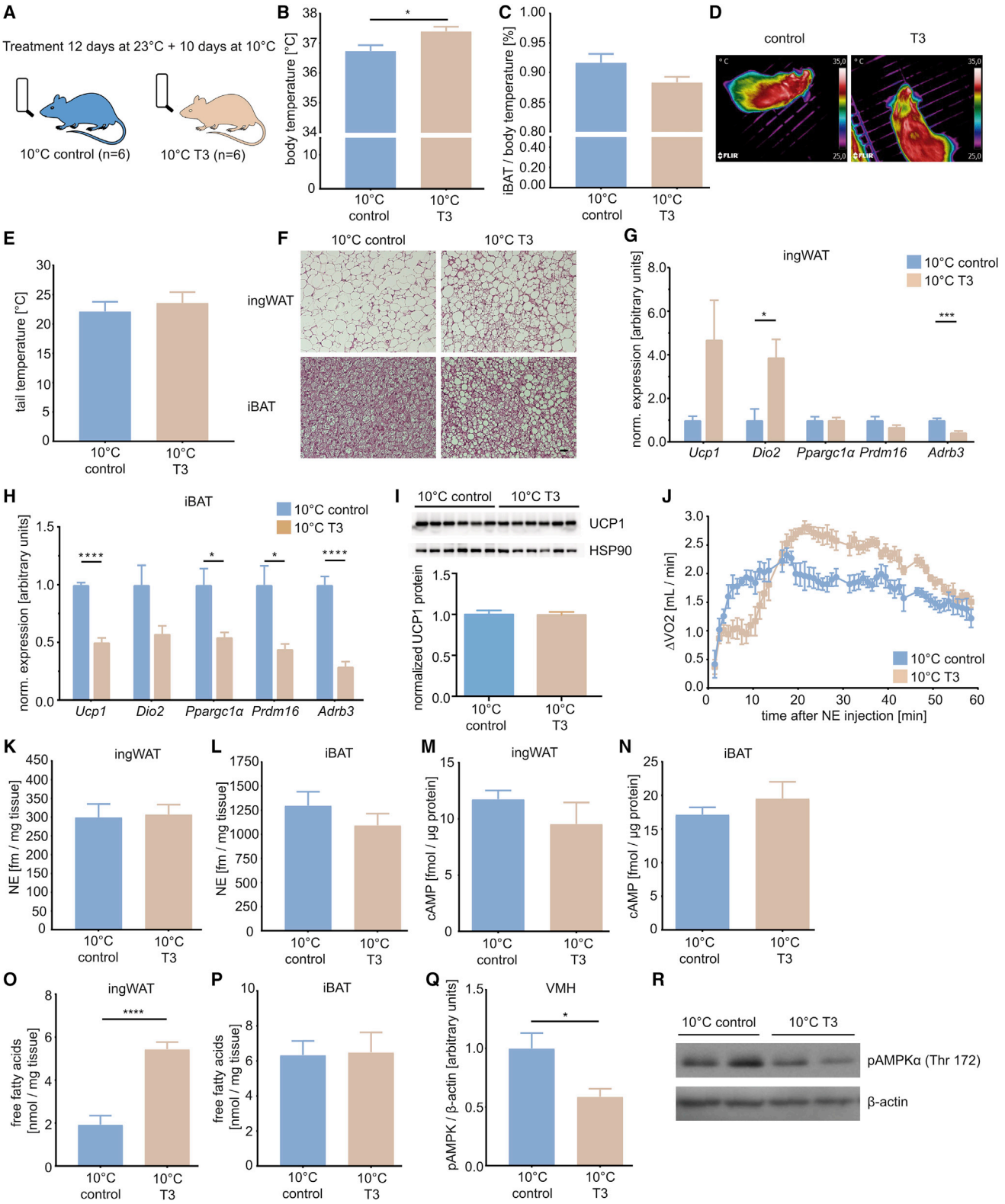

Figure 5. Thyroid-Hormone-Mediated Increase in Body Temperature Persists in the Cold

(A) Scheme of treatment regimen for induction of hyperthyroidism in WT mice at 23°C, following treatment at 10°C.

(B) Rectal temperature of control and T3-treated mice at the end of treatment at 10°C.

(legend continued on next page)

glucose and lipid uptake, as well as reduced iBAT surface temperature, both in absolute values as well as when normalized to body temperature—a mathematical way to compensate for the elevated temperature of the blood circulating through the BAT.

These findings of reduced metabolic activity in thermogenic fat are at first glance counterintuitive, as central hyperthyroidism in rats leads to iBAT activation through the SNS triggered by reduced AMPKα phosphorylation in the VMH (Alvarez-Crespo et al., 2016; López et al., 2010; Martínez-Sánchez et al., 2017b). However, when mice were treated with systemic T3 at 23°C and 30°C, no effect on AMPKα phosphorylation in the VMH was found, suggesting that the central T3 activation of iBAT thermogenesis may be blocked by an upstream thermostat. This seems plausible, as additional facultative thermogenesis is not required in the T3-treated mice at 23°C, because an excess of heat is already being produced and dissipated by the tail. Consequently, reduced AMPKα phosphorylation was only detected when the mice were exposed to cold during the T3 treatment, although the amount of hypothalamic T3 was comparable at 10°C, 23°C, or 30°C (not shown). Importantly, at 10°C the peripheral heat production is fully used to contribute to the maintenance of body temperature and does not cause hyperthermia as indicated by normal tail temperature. Therefore, the upstream block of the VMH seems to be released, allowing the expected central effect of T3 on the VMH. Most interestingly, cold-exposed T3-treated mice still had a higher body temperature, demonstrating that thyroid hormone also elevates the centrally defended body temperature. This suggests the coexistence of hyperthermia and pyrexia in T3-treated mice, with the hyperthermia prevailing at room temperature and above and the pyrexic phenotype appearing in the cold. It is now tempting to speculate that this simultaneous hyperthermic and pyrexic effect of thyroid hormone could have been an important factor in the evolutionary development of endothermy (Little and Seebacher, 2014).

The concept may also explain why ingWAT and iBAT are not activated despite their high UCP1 protein content in T3-treated mice: at 23°C and 30°C, the peripheral hyperthermia seems to be more than sufficient to maintain body temperature even at the elevated setpoint, and further facultative thermogenesis would not be beneficial. The apparent discrepancy between high UCP1 and not elevated thermogenesis concurs with previous findings, demonstrating that the mere presence of UCP1 is not sufficient for thermogenesis (Shabalina et al., 2010), and additional stimulation of the protein by free fatty acids is required to exploit the full thermogenic potential. In the T3-treated tissues, we did not detect such an increase in free fatty acids. Although SNS activity has not been measured directly, the lack of induction in intracellular cAMP suggests insufficient adrenergic stimulation, which may be partially explained by the reduced expression of *Adrb3* by T3 (Rubio et al., 1995; Silva, 2006). That the available UCP1 can be activated has been demonstrated by the NE stimulation of the T3-treated animals, which unleashed a strong increase in energy expenditure. It should be noted that *Ucp1* mRNA levels can be disconcordant with protein levels, presumably due to the relatively long half-life of the UCP1 protein (Puigserver et al., 1992), which has been observed here and in previous studies (Nedergaard and Cannon, 2013).

Our findings in UCP1 KO mice, which still display increased body temperature upon T3, finally confirmed that the effect is independent of brown or beige adipose tissue. Although other thermogenic mechanisms, like calcium or creatine cycling, exist (Ikeda et al., 2017; Kazak et al., 2015, 2017), they also do not seem to contribute to thermogenesis, as they were not induced on the mRNA level. This demonstrates that systemic treatment with thyroid hormone activates thermogenic pathways in tissues other than adipose depots (Silva, 2006). Given the elevated resting metabolic rate of T3-treated fasted mice at thermoneutrality, which under these conditions cannot result from any UCP1-mediated thermogenesis (Feldmann et al., 2009), as well as the increased lipid uptake and reduced glycogen content of M. Soleus and M. Gastrocnemius, respectively, it seems likely that the skeletal muscle is the source of the peripheral hyperthermia. This is supported by increased expression of genes and proteins involved in wasting cellular energy, such as *Ucp3*, *Gpd2*, or *Serca2* (Cannon and Nedergaard, 2010). Our findings are in concordance with previous studies, showing increased glucose turnover in skeletal muscle of hyperthyroid humans (Gavrila et al., 2017) and elevated fatty acid uptake in skeletal muscle of hyperthyroid rats (Klieverik et al., 2009). As muscle is predominantly TRα1 tissue, this would explain why a similar hyperthermia is not observed in mice treated with GC-1 (Lin et al., 2015).

In conclusion, our data demonstrate a strong and direct induction of browning of ingWAT in systemic hyperthyroidism in a TRβ-dependent manner. Although all classical features of browning, including the change in morphology and the increase in UCP1, are present, the beige fat does not contribute to whole-body metabolism or thermogenesis (Kalinovich et al., 2017; Nedergaard and Cannon, 2013; Shabalina et al., 2013). This is caused by the concomitant increase in basal metabolic rate mediated by TRα1 in muscle, which provides more heat than

(C) iBAT temperature as measured by infrared thermography at the end of treatment normalized to rectal temperature.
(D) Representative infrared (IR) pictures of control and T3-treated mice at the end of treatment at 10°C.
(E) Tail temperature of control and T3-treated mice at the end of treatment at 10°C.
(F) Representative H&E stainings of ingWAT and iBAT of WT mice housed and treated with T3 at 10°C. Scale bar 10 μm.
(G and H) Gene expression in (G) ingWAT and (H) iBAT of control and T3-treated mice at 10°C.
(I) UCP1 protein levels in iBAT of control and T3-treated mice housed and treated at 10°C.
(J) Change in oxygen consumption of control and T3-treated mice housed at 10°C after NE injection.
(K and L) NE content in (K) ingWAT and (L) iBAT of control and T3-treated mice at 10°C.
(M and N) cAMP levels in (M) ingWAT and (N) iBAT of mice housed and treated at 10°C.
(O and P) Quantification of free fatty acids in (O) ingWAT and (P) iBAT of mice housed and treated at 10°C.
(Q) Quantification of pAMPKα in the VMH of mice housed and treated with T3 at 10°C.
(R) Representative western blot of pAMPKα expression in the VMH of mice housed and treated with T3 at 10°C.
Data are presented as mean ± SEM; n = 6. *p < 0.05; **p < 0.01; ***p < 0.001. See also Figure S3.

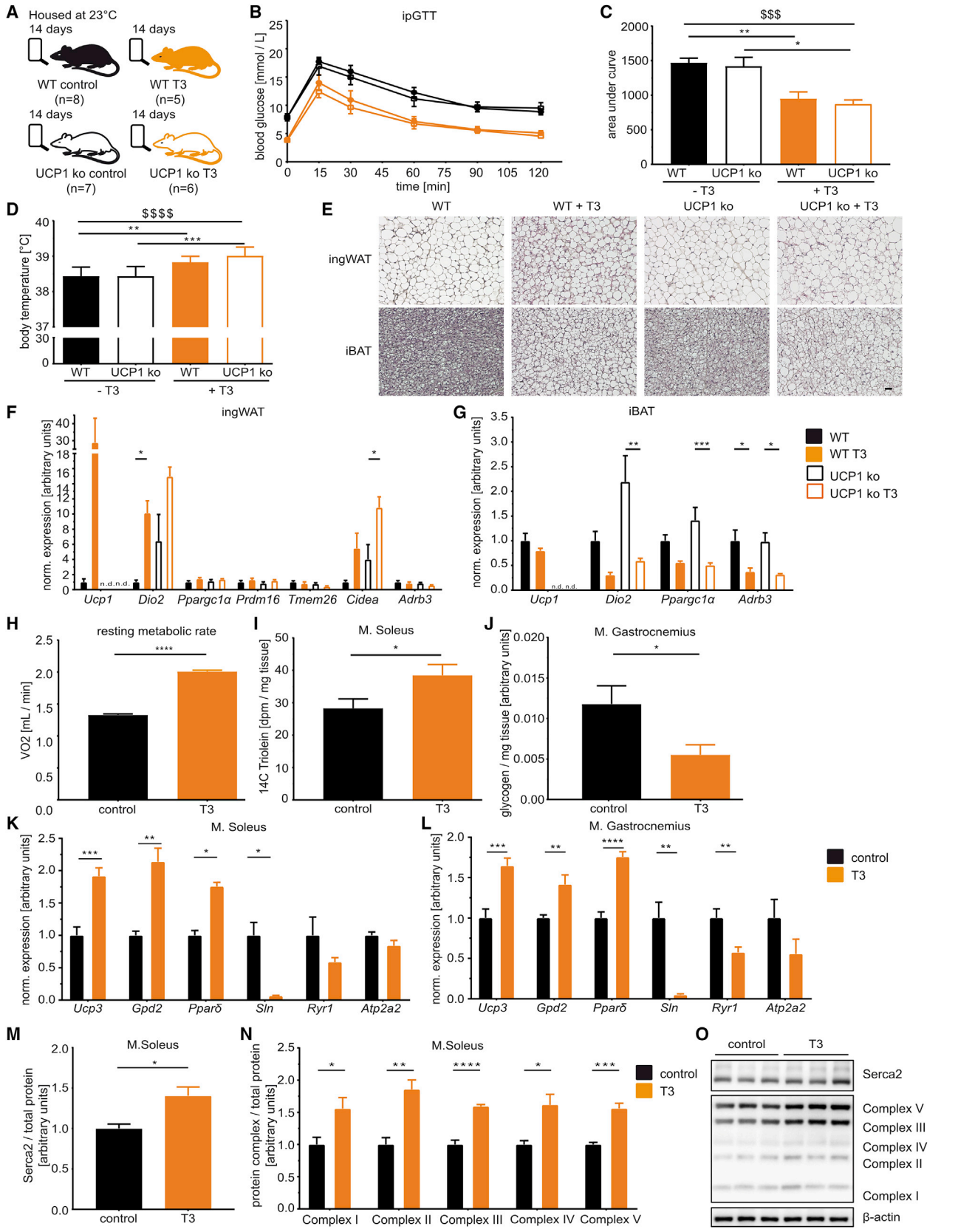

(legend on next page)

required to meet the simultaneously elevated setpoint, and consequently blocks further sympathetic activation by central mechanisms. Our findings thus demonstrate that the metabolic and thermogenic consequences of systemic hyperthyroidism do not rely on browning and that the mere presence of beige fat with detectable levels of UCP1 protein and other histological and molecular markers of browning does not necessarily translate to a metabolically active tissue. Therefore, a combination of techniques, including glucose and lipid turnover, as well as UCP1 KO mice should always be applied to validate the true thermogenic potential of the multiple other stimuli reported to induce browning (Castro et al., 2017; Tamucci et al., 2018; Vargas-Castillo et al., 2017; Warner and Mittag, 2016).

STAR★METHODS

Detailed methods are provided in the online version of this paper and include the following:

- KEY RESOURCES TABLE
- CONTACT FOR REAGENT AND RESOURCE SHARING
- EXPERIMENTAL MODEL AND SUBJECT DETAILS
- METHOD DETAILS
  - Study design
  - PET-CT
  - TRL Uptake
  - Indirect Calorimetry and nonshivering thermogenic capacity
  - NE turnover
  - Gene expression analysis
  - Western Blot
  - Enzyme activity and glycogen measurement
  - ELISA
  - Histology
- QUANTIFICATION AND STATISTICAL ANALYSIS

SUPPLEMENTAL INFORMATION

Supplemental Information can be found online at https://doi.org/10.1016/j.celrep.2019.05.054.

ACKNOWLEDGMENTS

We thank the animal caretakers at the GTH, the MPI Cologne, and the UKE Hamburg. This work was supported by grants of the Deutsche Forschungsgemeinschaft (MI1242/2-2 and 3-2 Heisenberg Program and MI1242/4-1 and 5-1 SPP1629 "Thyroid TransAct" to J.M.; AS547-1/1 to M.A.; GRK1957 "Adipocyte-Brain-Crosstalk"), Young Active Research in Endocrinology, Bioscientifica Trust (BT-000011), and European Society for Endocrinology to K.J. A.V.-P. and S.V. were funded by the BHF (RG/18/7/33636). M.L. was funded by Xunta de Galicia (2016-PG068) and Ministerio de Economía y Competitividad (MINECO) (SAF2015-71026-R). H.O. is a Lichtenberg Fellow of the Volkswagen Stiftung. We are grateful to Barbara Cannon and Jan Nedergaard for critical comments and fruitful scientific discussions and to An Ruiter for technical assistance.

AUTHOR CONTRIBUTIONS

K.J., J.R., S.N., and M.A. performed *in vivo* and *ex vivo* studies. K.J., A.L.C., L.H., and H.B. performed the PET-CT studies; A.W.F., M.H., and J.H. performed the TRL and ^{3}HDG uptake studies; S.V., A.W., A.V.-P., and J.W.D. helped with the NE turnover experiments; E.R.P. and M.L. performed the AMPK analyses; A.B. analyzed hypothalamic T3; K.J., R.O., G.B., H.O., M.L., and J.M. analyzed and discussed data; and K.J. and J.M. wrote the manuscript.

DECLARATION OF INTERESTS

The authors declare no competing interests.

Received: September 26, 2018
Revised: May 7, 2019
Accepted: May 15, 2019
Published: June 11, 2019

REFERENCES

Alvarez-Crespo, M., Csikasz, R.I., Martínez-Sánchez, N., Diéguez, C., Cannon, B., Nedergaard, J., and López, M. (2016). Essential role of UCP1 modulating the central effects of thyroid hormones on energy balance. Mol. Metab. *5*, 271–282.

Bartelt, A., and Heeren, J. (2014). Adipose tissue browning and metabolic health. Nat. Rev. Endocrinol. *10*, 24–36.

Bartelt, A., Bruns, O.T., Reimer, R., Hohenberg, H., Ittrich, H., Peldschus, K., Kaul, M.G., Tromsdorf, U.I., Weller, H., Waurisch, C., et al. (2011). Brown adipose tissue activity controls triglyceride clearance. Nat. Med. *17*, 200–205.

Bartelt, A., Widenmaier, S.B., Schlein, C., Johann, K., Goncalves, R.L.S., Eguchi, K., Fischer, A.W., Parlakgül, G., Snyder, N.A., Nguyen, T.B., et al. (2018). Brown adipose tissue thermogenic adaptation requires Nrf1-mediated proteasomal activity. Nat. Med. *24*, 292–303.

Berbée, J.F., Boon, M.R., Khedoe, P.P., Bartelt, A., Schlein, C., Worthmann, A., Kooijman, S., Hoeke, G., Mol, I.M., John, C., et al. (2015). Brown fat activation reduces hypercholesterolaemia and protects from atherosclerosis development. Nat. Commun. *6*, 6356.

Figure 6. Thyroid-Hormone-Mediated Increase in Body Temperature Is Independent of UCP1 Expression

(A) Scheme of treatment regimen for induction of hyperthyroidism in WT and UCP1 KO littermates.
(B) ipGTT of WT and UCP1 KO mice before and after treatment with T3 for 14 days. n = 5–6.
(C) Area under curve of ipGTT (B). n = 5–6.
(D) Rectal temperature of WT and UCP1 KO mice before and after treatment with T3 for 14 days. n = 5–6.
(E) Representative H&E stainings of ingWAT and iBAT of WT control, UCP1 KO control, T3-treated WT, and T3-treated UCP1 KO mice. Scale bar 10 μm.
(F and G) Gene expression analysis of (F) ingWAT and (G) iBAT of WT control, UCP1 KO control, T3-treated WT, and T3-treated UCP1 KO mice. n = 5–8.
(H) Resting metabolic rate at 30°C measured in mice housed and treated at 30°C. n = 5.
(I) Uptake of radioactively labeled TRLs into M. Soleus of control and T3-treated mice after 14 days of treatment at 23°C. n = 7–8.
(J) Glycogen content in M. Gastrocnemius of control and T3-treated mice at 23°C. n = 6–8.
(K and L) Gene expression in (K) M. Soleus and (L) M. Gastrocnemius of control and T3-treated mice at 23°C. n = 6–8.
(M) Serca2 protein expression in M. Soleus of control and T3-treated mice at 23°C. n = 6.
(N) Protein expression of complexes I–V of oxidative phosphorylation in M. Soleus of control and T3-treated mice at 23°C. n = 6.
(O) Representative western blot of Serca2 and complexes I–V in M. Soleus of control and T3-treated mice.
Data are presented as mean ± SEM. *p < 0.05; **p < 0.01; ***p < 0.001; $^{\$\$\$}p_{T3}$ < 0.001; $^{\$\$\$\$}p_{T3}$ < 0.0001. See also Figure S4.

Bianco, A.C., Anderson, G., Forrest, D., Galton, V.A., Gereben, B., Kim, B.W., Kopp, P.A., Liao, X.H., Obregon, M.J., Peeters, R.P., et al.; American Thyroid Association Task Force on Approaches and Strategies to Investigate Thyroid Hormone Economy and Action (2014). American Thyroid Association Guide to investigating thyroid hormone economy and action in rodent and cell models. Thyroid *24*, 88–168.

Cannon, B., and Nedergaard, J. (2004). Brown adipose tissue: function and physiological significance. Physiol. Rev. *84*, 277–359.

Cannon, B., and Nedergaard, J. (2010). Thyroid hormones: igniting brown fat via the brain. Nat. Med. *16*, 965–967.

Castro, É., Silva, T.E.O., and Festuccia, W.T. (2017). Critical review of beige adipocyte thermogenic activation and contribution to whole-body energy expenditure. Horm. Mol. Biol. Clin. Investig. *31*, /j/hmbci.2017.31.issue-2/hmbci-2017-0042/hmbci-2017-0042.xml.

Cheng, Y., Jiang, L., Keipert, S., Zhang, S., Hauser, A., Graf, E., Strom, T., Tschöp, M., Jastroch, M., and Perocchi, F. (2018). Prediction of Adipose Browning Capacity by Systematic Integration of Transcriptional Profiles. Cell Rep. *23*, 3112–3125.

Dalley, J.W., Theobald, D.E., Eagle, D.M., Passetti, F., and Robbins, T.W. (2002). Deficits in impulse control associated with tonically-elevated serotonergic function in rat prefrontal cortex. Neuropsychopharmacology *26*, 716–728.

Enerbäck, S., Jacobsson, A., Simpson, E.M., Guerra, C., Yamashita, H., Harper, M.E., and Kozak, L.P. (1997). Mice lacking mitochondrial uncoupling protein are cold-sensitive but not obese. Nature *387*, 90–94.

Feldmann, H.M., Golozoubova, V., Cannon, B., and Nedergaard, J. (2009). UCP1 ablation induces obesity and abolishes diet-induced thermogenesis in mice exempt from thermal stress by living at thermoneutrality. Cell Metab. *9*, 203–209.

Finan, B., Clemmensen, C., Zhu, Z., Stemmer, K., Gauthier, K., Müller, L., De Angelis, M., Moreth, K., Neff, F., Perez-Tilve, D., et al. (2016). Chemical hybridization of glucagon and thyroid hormone optimizes therapeutic impact for metabolic disease. Cell *167*, 843.

Fisher, F.M., Kleiner, S., Douris, N., Fox, E.C., Mepani, R.J., Verdeguer, F., Wu, J., Kharitonenkov, A., Flier, J.S., Maratos-Flier, E., and Spiegelman, B.M. (2012). FGF21 regulates PGC-1α and browning of white adipose tissues in adaptive thermogenesis. Genes Dev. *26*, 271–281.

Forrest, D., Hanebuth, E., Smeyne, R.J., Everds, N., Stewart, C.L., Wehner, J.M., and Curran, T. (1996). Recessive resistance to thyroid hormone in mice lacking thyroid hormone receptor beta: evidence for tissue-specific modulation of receptor function. EMBO J. *15*, 3006–3015.

Frederich, R.C., Hamann, A., Anderson, S., Löllmann, B., Lowell, B.B., and Flier, J.S. (1995). Leptin levels reflect body lipid content in mice: evidence for diet-induced resistance to leptin action. Nat. Med. *1*, 1311–1314.

Gavrila, A., Hasselgren, P.O., Glasgow, A., Doyle, A.N., Lee, A.J., Fox, P., Gautam, S., Hennessey, J.V., Kolodny, G.M., and Cypess, A.M. (2017). Variable Cold-Induced Brown Adipose Tissue Response to Thyroid Hormone Status. Thyroid *27*, 1–10.

Golozoubova, V., Gullberg, H., Matthias, A., Cannon, B., Vennström, B., and Nedergaard, J. (2004). Depressed thermogenesis but competent brown adipose tissue recruitment in mice devoid of all hormone-binding thyroid hormone receptors. Mol. Endocrinol. *18*, 384–401.

Greco-Perotto, R., Zaninetti, D., Assimacopoulos-Jeannet, F., Bobbioni, E., and Jeanrenaud, B. (1987). Stimulatory effect of cold adaptation on glucose utilization by brown adipose tissue. Relationship with changes in the glucose transporter system. J. Biol. Chem. *262*, 7732–7736.

Hankir, M.K., Kranz, M., Keipert, S., Weiner, J., Andreasen, S.G., Kern, M., Patt, M., Klöting, N., Heiker, J.T., Brust, P., et al. (2017). Dissociation Between Brown Adipose Tissue ^{18}F-FDG Uptake and Thermogenesis in Uncoupling Protein 1-Deficient Mice. J. Nucl. Med. *58*, 1100–1103.

Harms, M., and Seale, P. (2013). Brown and beige fat: development, function and therapeutic potential. Nat. Med. *19*, 1252–1263.

Heine, M., Fischer, A.W., Schlein, C., Jung, C., Straub, L.G., Gottschling, K., Mangels, N., Yuan, Y., Nilsson, S.K., Liebscher, G., et al. (2018). Lipolysis Triggers a Systemic Insulin Response Essential for Efficient Energy Replenishment of Activated Brown Adipose Tissue in Mice. Cell Metab. *28*, 644–655.e4.

Hoefig, C.S., Harder, L., Oelkrug, R., Meusel, M., Vennström, B., Brabant, G., and Mittag, J. (2016). Thermoregulatory and Cardiovascular Consequences of a Transient Thyrotoxicosis and Recovery in Male Mice. Endocrinology *157*, 2957–2967.

Hotta, Y., Nakamura, H., Konishi, M., Murata, Y., Takagi, H., Matsumura, S., Inoue, K., Fushiki, T., and Itoh, N. (2009). Fibroblast growth factor 21 regulates lipolysis in white adipose tissue but is not required for ketogenesis and triglyceride clearance in liver. Endocrinology *150*, 4625–4633.

Husse, J., Hintze, S.C., Eichele, G., Lehnert, H., and Oster, H. (2012). Circadian clock genes Per1 and Per2 regulate the response of metabolism-associated transcripts to sleep disruption. PLoS ONE *7*, e52983.

Ikeda, K., Kang, Q., Yoneshiro, T., Camporez, J.P., Maki, H., Homma, M., Shinoda, K., Chen, Y., Lu, X., Maretich, P., et al. (2017). UCP1-independent signaling involving SERCA2b-mediated calcium cycling regulates beige fat thermogenesis and systemic glucose homeostasis. Nat. Med. *23*, 1454–1465.

Inagaki, T., Dutchak, P., Zhao, G., Ding, X., Gautron, L., Parameswara, V., Li, Y., Goetz, R., Mohammadi, M., Esser, V., et al. (2007). Endocrine regulation of the fasting response by PPARalpha-mediated induction of fibroblast growth factor 21. Cell Metab. *5*, 415–425.

Ishibashi, J., and Seale, P. (2010). Medicine. Beige can be slimming. Science *328*, 1113–1114.

Jais, A., Solas, M., Backes, H., Chaurasia, B., Kleinridders, A., Theurich, S., Mauer, J., Steculorum, S.M., Hampel, B., Goldau, J., et al. (2016). Myeloid-Cell-Derived VEGF Maintains Brain Glucose Uptake and Limits Cognitive Impairment in Obesity. Cell *165*, 882–895.

Jastroch, M., Hirschberg, V., and Klingenspor, M. (2012). Functional characterization of UCP1 in mammalian HEK293 cells excludes mitochondrial uncoupling artefacts and reveals no contribution to basal proton leak. Biochim. Biophys. Acta *1817*, 1660–1670.

Kajimura, S., Spiegelman, B.M., and Seale, P. (2015). Brown and Beige Fat: Physiological Roles beyond Heat Generation. Cell Metab. *22*, 546–559.

Kalinovich, A.V., de Jong, J.M., Cannon, B., and Nedergaard, J. (2017). UCP1 in adipose tissues: two steps to full browning. Biochimie *134*, 127–137.

Kazak, L., Chouchani, E.T., Jedrychowski, M.P., Erickson, B.K., Shinoda, K., Cohen, P., Vetrivelan, R., Lu, G.Z., Laznik-Bogoslavski, D., Hasenfuss, S.C., et al. (2015). A creatine-driven substrate cycle enhances energy expenditure and thermogenesis in beige fat. Cell *163*, 643–655.

Kazak, L., Chouchani, E.T., Lu, G.Z., Jedrychowski, M.P., Bare, C.J., Mina, A.I., Kumari, M., Zhang, S., Vuckovic, I., Laznik-Bogoslavski, D., et al. (2017). Genetic depletion of adipocyte creatine metabolism inhibits diet-induced thermogenesis and drives obesity. Cell Metab. *26*, 693.

Keipert, S., and Jastroch, M. (2014). Brite/beige fat and UCP1 - is it thermogenesis? Biochim. Biophys. Acta *1837*, 1075–1082.

Kharitonenkov, A., Shiyanova, T.L., Koester, A., Ford, A.M., Micanovic, R., Galbreath, E.J., Sandusky, G.E., Hammond, L.J., Moyers, J.S., Owens, R.A., et al. (2005). FGF-21 as a novel metabolic regulator. J. Clin. Invest. *115*, 1627–1635.

Klieverik, L.P., Coomans, C.P., Endert, E., Sauerwein, H.P., Havekes, L.M., Voshol, P.J., Rensen, P.C., Romijn, J.A., Kalsbeek, A., and Fliers, E. (2009). Thyroid hormone effects on whole-body energy homeostasis and tissue-specific fatty acid uptake in vivo. Endocrinology *150*, 5639–5648.

Lin, J.Z., Martagón, A.J., Cimini, S.L., Gonzalez, D.D., Tinkey, D.W., Biter, A., Baxter, J.D., Webb, P., Gustafsson, J.A., Hartig, S.M., and Phillips, K.J. (2015). Pharmacological Activation of Thyroid Hormone Receptors Elicits a Functional Conversion of White to Brown Fat. Cell Rep. *13*, 1528–1537.

Little, A.G., and Seebacher, F. (2014). The evolution of endothermy is explained by thyroid hormone-mediated responses to cold in early vertebrates. J. Exp. Biol. *217*, 1642–1648.

López, M., Varela, L., Vázquez, M.J., Rodríguez-Cuenca, S., González, C.R., Velagapudi, V.R., Morgan, D.A., Schoenmakers, E., Agassandian, K., Lage, R., et al. (2010). Hypothalamic AMPK and fatty acid metabolism mediate thyroid regulation of energy balance. Nat. Med. *16*, 1001–1008.

López, M., Alvarez, C.V., Nogueiras, R., and Diéguez, C. (2013). Energy balance regulation by thyroid hormones at central level. Trends Mol. Med. *19*, 418–427.

Martínez-Sánchez, N., Moreno-Navarrete, J.M., Contreras, C., Rial-Pensado, E., Fernø, J., Nogueiras, R., Diéguez, C., Fernández-Real, J.M., and López, M. (2017a). Thyroid hormones induce browning of white fat. J. Endocrinol. *232*, 351–362.

Martínez-Sánchez, N., Seoane-Collazo, P., Contreras, C., Varela, L., Villarroya, J., Rial-Pensado, E., Buqué, X., Aurrekoetxea, I., Delgado, T.C., Vázquez-Martínez, R., et al. (2017b). Hypothalamic AMPK-ER stress-JNK1 axis mediates the central actions of thyroid hormones on energy balance. Cell Metab. *26*, 212–229.e12.

Mullur, R., Liu, Y.Y., and Brent, G.A. (2014). Thyroid hormone regulation of metabolism. Physiol. Rev. *94*, 355–382.

Nedergaard, J., and Cannon, B. (2013). UCP1 mRNA does not produce heat. Biochim. Biophys. Acta *1831*, 943–949.

Neilsen, E.L. (1953). Studies on hereditary dwarfism in mice. XIV. Effect of thyroxin and growth hormone on growth. Acta Pathol. Microbiol. Scand. *32*, 316–334.

Olsen, J.M., Csikasz, R.I., Dehvari, N., Lu, L., Sandström, A., Öberg, A.I., Nedergaard, J., Stone-Elander, S., and Bengtsson, T. (2017). β_3-Adrenergically induced glucose uptake in brown adipose tissue is independent of UCP1 presence or activity: Mediation through the mTOR pathway. Mol. Metab. *6*, 611–619.

Oster, H., Damerow, S., Hut, R.A., and Eichele, G. (2006). Transcriptional profiling in the adrenal gland reveals circadian regulation of hormone biosynthesis genes and nucleosome assembly genes. J. Biol. Rhythms *21*, 350–361.

Petrovic, N., Walden, T.B., Shabalina, I.G., Timmons, J.A., Cannon, B., and Nedergaard, J. (2010). Chronic peroxisome proliferator-activated receptor gamma (PPARgamma) activation of epididymally derived white adipocyte cultures reveals a population of thermogenically competent, UCP1-containing adipocytes molecularly distinct from classic brown adipocytes. J. Biol. Chem. *285*, 7153–7164.

Puigserver, P., Herron, D., Gianotti, M., Palou, A., Cannon, B., and Nedergaard, J. (1992). Induction and degradation of the uncoupling protein thermogenin in brown adipocytes in vitro and in vivo. Evidence for a rapidly degradable pool. Biochem. J. *284*, 393–398.

Rabelo, R., Schifman, A., Rubio, A., Sheng, X., and Silva, J.E. (1995). Delineation of thyroid hormone-responsive sequences within a critical enhancer in the rat uncoupling protein gene. Endocrinology *136*, 1003–1013.

Rabelo, R., Reyes, C., Schifman, A., and Silva, J.E. (1996). Interactions among receptors, thyroid hormone response elements, and ligands in the regulation of the rat uncoupling protein gene expression by thyroid hormone. Endocrinology *137*, 3478–3487.

Rakov, H., Engels, K., Hönes, G.S., Strucksberg, K.H., Moeller, L.C., Köhrle, J., Zwanziger, D., and Führer, D. (2016). Sex-specific phenotypes of hyperthyroidism and hypothyroidism in mice. Biol. Sex Differ. *7*, 36.

Ribeiro, M.O., Carvalho, S.D., Schultz, J.J., Chiellini, G., Scanlan, T.S., Bianco, A.C., and Brent, G.A. (2001). Thyroid hormone–sympathetic interaction and adaptive thermogenesis are thyroid hormone receptor isoform–specific. J. Clin. Invest. *108*, 97–105.

Green, E.L. (1975). Biology of the Laboratory Mouse (Dover Publications).

Rubio, A., Raasmaja, A., and Silva, J.E. (1995). Thyroid hormone and norepinephrine signaling in brown adipose tissue. II: Differential effects of thyroid hormone on beta 3-adrenergic receptors in brown and white adipose tissue. Endocrinology *136*, 3277–3284.

Salvatore, D., Simonides, W.S., Dentice, M., Zavacki, A.M., and Larsen, P.R. (2014). Thyroid hormones and skeletal muscle–new insights and potential implications. Nat. Rev. Endocrinol. *10*, 206–214.

Santhanam, P., Ahima, R.S., Mammen, J.S., Giovanella, L., and Treglia, G. (2018). Brown adipose tissue (BAT) detection by 18F-FDG PET and thyroid hormone level(s)-a systematic review. Endocrine *62*, 496–500.

Sap, J., Muñoz, A., Damm, K., Goldberg, Y., Ghysdael, J., Leutz, A., Beug, H., and Vennström, B. (1986). The c-erb-A protein is a high-affinity receptor for thyroid hormone. Nature *324*, 635–640.

Shabalina, I.G., Ost, M., Petrovic, N., Vrbacky, M., Nedergaard, J., and Cannon, B. (2010). Uncoupling protein-1 is not leaky. Biochim. Biophys. Acta *1797*, 773–784.

Shabalina, I.G., Petrovic, N., de Jong, J.M., Kalinovich, A.V., Cannon, B., and Nedergaard, J. (2013). UCP1 in brite/beige adipose tissue mitochondria is functionally thermogenic. Cell Rep. *5*, 1196–1203.

Shibata, H., Pérusse, F., Vallerand, A., and Bukowiecki, L.J. (1989). Cold exposure reverses inhibitory effects of fasting on peripheral glucose uptake in rats. Am. J. Physiol. *257*, R96–R101.

Silva, J.E. (2003). The thermogenic effect of thyroid hormone and its clinical implications. Ann. Intern. Med. *139*, 205–213.

Silva, J.E. (2006). Thermogenic mechanisms and their hormonal regulation. Physiol. Rev. *86*, 435–464.

Silva, J.E., and Larsen, P.R. (1983). Adrenergic activation of triiodothyronine production in brown adipose tissue. Nature *305*, 712–713.

Sjögren, M., Alkemade, A., Mittag, J., Nordström, K., Katz, A., Rozell, B., Westerblad, H., Arner, A., and Vennström, B. (2007). Hypermetabolism in mice caused by the central action of an unliganded thyroid hormone receptor alpha1. EMBO J. *26*, 4535–4545.

Svensson, K.J., Long, J.Z., Jedrychowski, M.P., Cohen, P., Lo, J.C., Serag, S., Kir, S., Shinoda, K., Tartaglia, J.A., Rao, R.R., et al. (2016). A secreted Slit2 fragment regulates adipose tissue thermogenesis and metabolic function. Cell Metab. *23*, 454–466.

Tamucci, K.A., Namwanje, M., Fan, L., and Qiang, L. (2018). The dark side of browning. Protein Cell *9*, 152–163.

Tata, J.R. (1986). The search for the mechanism of hormone action. Perspect. Biol. Med. *29*, S184–S204.

Thompson, C.C., Weinberger, C., Lebo, R., and Evans, R.M. (1987). Identification of a novel thyroid hormone receptor expressed in the mammalian central nervous system. Science *237*, 1610–1614.

Vargas-Castillo, A., Fuentes-Romero, R., Rodriguez-Lopez, L.A., Torres, N., and Tovar, A.R. (2017). Understanding the biology of thermogenic fat: is browning a new approach to the treatment of obesity? Arch. Med. Res. *48*, 401–413.

Vujovic, M., Nordström, K., Gauthier, K., Flamant, F., Visser, T.J., Vennström, B., and Mittag, J. (2009). Interference of a mutant thyroid hormone receptor alpha1 with hepatic glucose metabolism. Endocrinology *150*, 2940–2947.

Warner, A., and Mittag, J. (2012). Thyroid hormone and the central control of homeostasis. J. Mol. Endocrinol. *49*, R29–R35.

Warner, A., and Mittag, J. (2016). Breaking BAT: can browning create a better white? J. Endocrinol. *228*, R19–R29.

Warner, A., Rahman, A., Solsjö, P., Gottschling, K., Davis, B., Vennström, B., Arner, A., and Mittag, J. (2013). Inappropriate heat dissipation ignites brown fat thermogenesis in mice with a mutant thyroid hormone receptor α1. Proc. Natl. Acad. Sci. USA *110*, 16241–16246.

Weiner, J., Kranz, M., Klöting, N., Kunath, A., Steinhoff, K., Rijntjes, E., Köhrle, J., Zeisig, V., Hankir, M., Gebhardt, C., et al. (2016). Thyroid hormone status defines brown adipose tissue activity and browning of white adipose tissues in mice. Sci. Rep. *6*, 38124.

Weiss, R.E., Murata, Y., Cua, K., Hayashi, Y., Seo, H., and Refetoff, S. (1998). Thyroid hormone action on liver, heart, and energy expenditure

in thyroid hormone receptor beta-deficient mice. Endocrinology *139*, 4945–4952.

Yen, P.M. (2001). Physiological and molecular basis of thyroid hormone action. Physiol. Rev. *81*, 1097–1142.

Young, P., Arch, J.R., and Ashwell, M. (1984). Brown adipose tissue in the parametrial fat pad of the mouse. FEBS Lett. *167*, 10–14.

Zhang, Z., Bisschop, P.H., Foppen, E., van Beeren, H.C., Kalsbeek, A., Boelen, A., and Fliers, E. (2016). A model for chronic, intrahypothalamic thyroid hormone administration in rats. J. Endocrinol. *229*, 37–45.

Zhao, J., Unelius, L., Bengtsson, T., Cannon, B., and Nedergaard, J. (1994). Coexisting beta-adrenoceptor subtypes: significance for thermogenic process in brown fat cells. Am. J. Physiol. *267*, C969–C979.

STAR★METHODS

KEY RESOURCES TABLE

REAGENT or RESOURCE	SOURCE	IDENTIFIER
Antibodies		
anti-UCP1	Jastroch et al., 2012	N/A
anti-Serca2	Cell Signaling Technology	Cat#4388; RRID:AB_2227684
anti-HSL	Cell Signaling Technology	Cat#4107; RRID:AB_2296900
anti-pHSL(Ser660)	Cell Signaling Technology	Cat#4126S; RRID:AB_490997
anti-OxPhos cocktail	Invitrogen	Cat#45-8099; RRID:AB_2533835
anti-Tyrosine Hydroxylase	Sigma	Cat#C2928
anti-β-actin	Sigma	Cat#A1978; RRID:AB_476692
anti-HSP90	Cell Signaling Technology	Cat#4877; RRID:AB_2233307
anti-pAMPKα(Thr172)	Cell Signaling Technology	Cat#2535; RRID:AB_331250
anti-β-actin(AC-74)	Sigma	Cat#A5316; RRID:AB_476743
anti-rabbit polyclonal HRP-conjugated antibody	DAKO, Denmark	Cat#P0448; RRID:AB_2617138
anti-mouse polyclonal HRP-conjugated antibody	DAKO, Denmark	Cat#P0447; RRID:AB_2617137
Chemicals, Peptides, and Recombinant Proteins		
L-Thyroxine (T4)	Sigma Aldrich, Germany	Cat#T2376
3,3′,5-Triiodo-L-thyronine (T3)	Sigma Aldrich, Germany	Cat#T6397
Arterenol (Norepinephrine)	Sanofi	Cat#03870227
α-methyl-DL-tyrosine methyl ester hydrochloride (AMPT)	Sigma Aldrich, Germany	Cat#M3281
Critical Commercial Assays		
Pierce BCA Kit	Thermo Scientific, Germany	Cat#23227
TGX Stain Free FastCast Acrylamide Kit	Bio-Rad Laboratories, Germany	Cat#1610183, Cat#1610185
Advansta WesternBright Quantum	Advansta, USA	Cat#K-12041-D20
Serum total T4	DRG Diagnostics, Germany	Cat#EIA-1781
Serum total T3	NovaTec Immundiagnostica GmbH, Germany	Cat#DNOV053
Amersham cAMP Biotrak EIA	GE Healthcare Life Sciences	Cat#RPN225
Free Fatty Acid Quantification Kit	abcam plc, UK	Cat#ab65341
Experimental Models: Organisms/Strains		
C57BL/6NCr	Charles River Laboratories, Germany	RRID:MGI:2160593
B6.129S1-Thrbtm1Df/J (TRβ ko)	Forrest et al., 1996	RRID:IMSR_JAX:003462
B6.129-UCP1tmKZ/J (UCP1 ko)	Enerbäck et al., 1997	N/A
Per 1/2 dko	Husse et al., 2012	N/A
Oligonucleotides		
Primer sequences see Table S3		N/A
Software and Algorithms		
Phenomaster software	TSE Systems, Germany	N/A
Minispec Plus Software 6.0	Bruker Corp., Billerica, MA, USA	N/A
Microsoft Office Excel 2013	Microsoft	N/A
Prism 7	GraphPad	N/A
CircWave v.1.4	Oster et al., 2006	N/A

CONTACT FOR REAGENT AND RESOURCE SHARING

Further information and requests for resources and reagents should be directed to and will be fulfilled by the Lead Contact Prof. Dr. Jens Mittag (jens.mittag@uni-luebeck.de).

EXPERIMENTAL MODEL AND SUBJECT DETAILS

Unless stated otherwise, animals were housed in groups at 23 ± 1°C at constant 12 hour light/dark cycle with *ad libitum* access to food and water. Experiments were conducted in male mice at the age of three to six months. Wild-type C57/BL6NCr (RRID:MGI:2160593) were purchased from Charles River Laboratories (Charles River, Germany), TRβ ko mice (RRID:IMSR_JAX:003462), UCP1 ko mice and Per1/Per2 dko mice were generated as described before (Enerbäck et al., 1997; Forrest et al., 1996; Husse et al., 2012) and knockout mice were always compared to WT littermate controls. All animal procedures were approved by the MELUR Schleswig-Holstein, LANUV Nordrhein-Westfalen and the BGV Hamburg, Germany.

METHOD DETAILS

Study design

Hyperthyroidism was induced by treatment with THs in drinking water as recommended by the American Thyroid Association guidelines with a dose low enough to avoid cachexia (Bianco et al., 2014), i.e., 1 mg/L L-Thyroxine (T2376, Sigma Aldrich, Germany) in 0.01% BSA (A7906, Sigma Aldrich, Germany) or 0.5 mg/L 3,3′,5-Triiodo-L-thyronine (T6397, Sigma Aldrich, Germany) in 0.01% BSA for 14 days (Figure 1A). Control mice received 0.01% BSA. Basic metabolic profiling was performed by measuring body weight, food and water intake, measurement of core body temperature using a rectal probe (BAT-12, Physitemp, USA), infrared thermography (T335, FLIR, Sweden) (Warner et al., 2013), and glucose tolerance tests (ipGTT, 2 g/kg body weight). Body composition was measured using Minispec LF110 and Minispec Plus Software 6.0 (Bruker Corp., Billerica, MA, USA). Organ collection was always performed in the middle of the light phase, unless stated otherwise.

PET-CT

[^{18}F]-FDG PET imaging and kinetic modeling was performed as described before (Jais et al., 2016). For the analysis of the parametric images of the metabolic rate of glucose (MRglc) volumes of interests (VOIs) containing iBAT or ingWAT, respectively were defined for each individual animal and each measurement.

TRL Uptake

Uptake of triglyceride-rich lipoproteins and [^{3}H]2-Deoxyglucose (^{3}HDG) in hyperthyroid C57/BL6NCr mice was investigated as described before (Bartelt et al., 2011). Briefly, mice were fasted for 4 hr before receiving an intravenous injection of 100 μL radiolabelled recombinant TRLs (80 mg triglycerides/kg) labeled with ^{14}C-triolein (0.6 MBq/kg) and ^{3}HDG. Organs from anesthetized mice were harvested after systemic perfusion with PBS-heparin (10 U/ml) via the left heart ventricle. Tissues were homogenized using Solvable (Perkin Elmer) and radioactivity was determined using liquid scintillation counting.

Indirect Calorimetry and nonshivering thermogenic capacity

Measurements of daily energy expenditure and basal metabolic rate in WT and TRβ ko littermates was performed in single-housed animals using Phenomaster (TSE Systems, Germany). Oxygen consumption (VO_2), carbon dioxide production (VCO_2), respiratory exchange rate (RQ), and energy expenditure (EE) were calculated with Microsoft Office Excel and Phenomaster software (TSE Systems, Germany). Basal metabolic rate was measured for 1 hour in animals fasted for 6 hours at 30°C.

Energy expenditure, respiratory exchange rate and nonshivering thermogenic capacity in fasted control and T3-treated mice were performed using the CaloBox system (PhenoSys GmbH, Germany). For measurement of daily energy expenditure at 23°C and resting metabolic rate at 30°C, mice were acclimated to the chambers individually for at least 60 minutes, before basal O_2 consumption and CO_2 production was analyzed for up to 60 minutes in 20 s intervals. For analysis of nonshivering thermogenesis capacity in mice housed and treated at 10°C or 23°C, respectively, mice were acclimated to chambers for at least 60 minutes. Then basal energy expenditure at 23°C was measured for 30 minutes, before injecting mice subcutaneously with 1 mg/kg NE (Arterenol, Sanofi) and measuring O_2 consumption and CO_2 production in intervals of 20 s for at least 60 minutes after injection. The change in oxygen consumption (ΔVO_2) was calculated by subtracting basal O_2 consumption before NE injection from O_2 consumption after NE injection.

NE turnover

In order to determine NE turnover in hyperthyroid WT mice, n = 16 mice per group were treated for two weeks with T3 or T4, respectively. On the last day of treatment mice were injected with the tyrosine hydroxylase inhibitor α-methyl-DL-tyrosine methyl ester hydrochloride (i.p. 120 mg/kg) (AMPT, M3281, Sigma Aldrich, Germany) and sacrificed after 0, 2, 4 and 6 hours (n = 4 per group and time point), respectively. Catecholamines were extracted in 2% perchloric acid (PCA, 48%–50%, 44464, Alfa Aesar, MA, USA) and quantified as described before (Dalley et al., 2002). Protein content of the samples was quantified using DC Protein Assay Kit according to manufacturer's protocol (Bio-Rad Laboratories, Inc.).

Gene expression analysis

For gene expression analysis, RNA was isolated using QIAGEN RNeasy Kits (QIAGEN, Germany), transcribed into cDNA (Molecular Biology RevertAid Strand cDNA Kit, Thermo Fisher Scientific, Germany) following manufacturer's instructions. qPCR analysis was

performed using SYBR Green PCR Master Mix (Roche, Germany) and QuantStudio Applied Biosystems (Thermo Fisher Scientific, Germany). Efficiency of the PCR was calculated using standard curves and levels of gene expression were normalized to a housekeeping gene (*ribosomal protein lateral stalk subunit P0*, *Rplp0* and *peptidylprolyl isomerase a*, *Ppia* for adipose tissues; *Ppia* and *hypoxanthine phosphoribosyltransferase*, *Hprt* for M. Soleus and M.Gastrocnemius, and *Hprt* for pituitary and hypothalamus) using the $\Delta\Delta C_T$ method. Primer sequences are listed in Table S3.

Western Blot

Protein isolation from snap-frozen tissue was performed by homogenizing tissues in RIPA buffer (150 mM NaCl, 50 mM Tris-HCl pH 7.5, 0.1% wt/vol SDS, 0.5% wt/vol sodium deoxycholate, 1% vol/vol Nonidet P40, 1 mM EDTA, 1 mM EGTA, 2.5 mM sodium pyrophosphate, 1 mM $NaVO_4$ and 10 mM NaF), with freshly added Protease inhibitors (5892970001, Roche Diagnostics GmbH, Germany). Protein concentration was determined using Pierce BCA Kit (23227, Thermo Scientific, Germany). Electrophoresis was performed using SDS Gels (TGX Stain Free FastCast Acrylamide Kit (1610183, 1610185, Bio-Rad Laboratories, Germany). Proteins were then transferred onto PVDF membrane (IPVH00010, Merck Millipore, Ltd, Cork, Ireland), blocked for 1 hour in 5% milk in TBS-T and incubated with primary antibodies (anti-UCP1; Jastroch et al., 2012); anti-Serca2, 4388, Cell Signaling Technology, Inc.; anti-HSL, 4107, Cell Signaling Technology, Inc.; anti-pHSL(Ser660), 4126S, Cell Signaling Technology, Inc.; anti-OxPhos cocktail, 45-8099, Invitrogen; anti-Tyrosine Hydroxylase, C2928, Sigma; anti-β-actin, A1978, Sigma; anti-HSP90, 4877, Cell Signaling Technology, Inc.) for 16 hours at 4°C. Afterward membranes were washed 4x10 minutes, incubated with secondary antibodies (anti-rabbit polyclonal HRP-conjugated antibody, P0448, DAKO, Denmark; anti-mouse polyclonal HRP-conjugated antibody, P0447, DAKO, Denmark) for 1 hour at room temperature, and washed again for 4x10 minutes. Chemiluminescence was recorded using Advansta WesternBright Quantum (K-12041-D20, Advansta, USA) and ChemiDoc Touch Imaging System (Bio-Rad Laboratories, Germany). Quantification of band intensities was performed using ImageLab™ Software (Bio-Rad Laboratories, Germany). Protein expression analysis in the VMH (anti-pAMPKα(Thr172), 2535, Cell Signaling Technology, Inc.; anti-β-actin(AC-74), A5316, Sigma) was performed as described before (Alvarez-Crespo et al., 2016). Protein expression was normalized to total protein content transferred onto the membrane, or housekeeping proteins, respectively.

Enzyme activity and glycogen measurement

Glycogen content in liver and M. Gastrocnemius, as well as activities of Pyruvate Kinase and hepatic Phosphoenolpyruvate Carboxykinase of snap-frozen tissue were determined as described before (Vujovic et al., 2009).

ELISA

Serum levels of tT4 (EIA-1781, DRG Diagnostics, Germany) and tT3 (DNOV053, NovaTec Immundiagnostica GmbH, Germany) were determined according to manufacturer's instructions. Hypothalamic T3 content was measured in pooled hypothalamic punches of the lateral and basal hypothalamus as described previously (Zhang et al., 2016). cAMP levels in ingWAT and iBAT were determined according to manufacturer's instructions (RPN225, GE Healthcare, UK). Free fatty acids in ingWAT and iBAT samples were analyzed according to manufacturer's instructions (ab65341, abcam plc; UK).

Histology

Tissues were fixed in 4% paraformaldehyde for 48 hours, dehydrated by washing in increasing concentrations of ethanol and xylol before embedding into paraffin. Tissues were cut in 5 μm slides and stained with Hemalun and Eosin according to the manufacturer's protocol (X883.2, T865.3, Carl Roth GmbH&Co KG, Germany).

QUANTIFICATION AND STATISTICAL ANALYSIS

For analysis of all data Microsoft Office Excel and GraphPad Prism 7 software was used. Analysis of circadian rhythms was performed using CircWave v.1.4 software (Oster et al., 2006). The variances between groups investigated were similar and appropriate tests were performed to analyze differences between the respective groups. For experiments with repeated-measurements a RM ANOVA was performed with individual post-tests, the experiments of the UCP1 ko mice and T3 treatment were analyzed using a 2-WAY ANOVA with post-tests. All values are represented as mean ± SEM. Number of animals (n) per experiment are depicted in each figure.

Cell Reports, Volume *27*

Supplemental Information

Thyroid-Hormone-Induced Browning of White Adipose Tissue Does Not Contribute to Thermogenesis and Glucose Consumption

Kornelia Johann, Anna Lena Cremer, Alexander W. Fischer, Markus Heine, Eva Rial Pensado, Julia Resch, Sebastian Nock, Samuel Virtue, Lisbeth Harder, Rebecca Oelkrug, Mariana Astiz, Georg Brabant, Amy Warner, Antonio Vidal-Puig, Henrik Oster, Anita Boelen, Miguel López, Joerg Heeren, Jeffrey W. Dalley, Heiko Backes, and Jens Mittag

Figure S1, Related to Figure 1

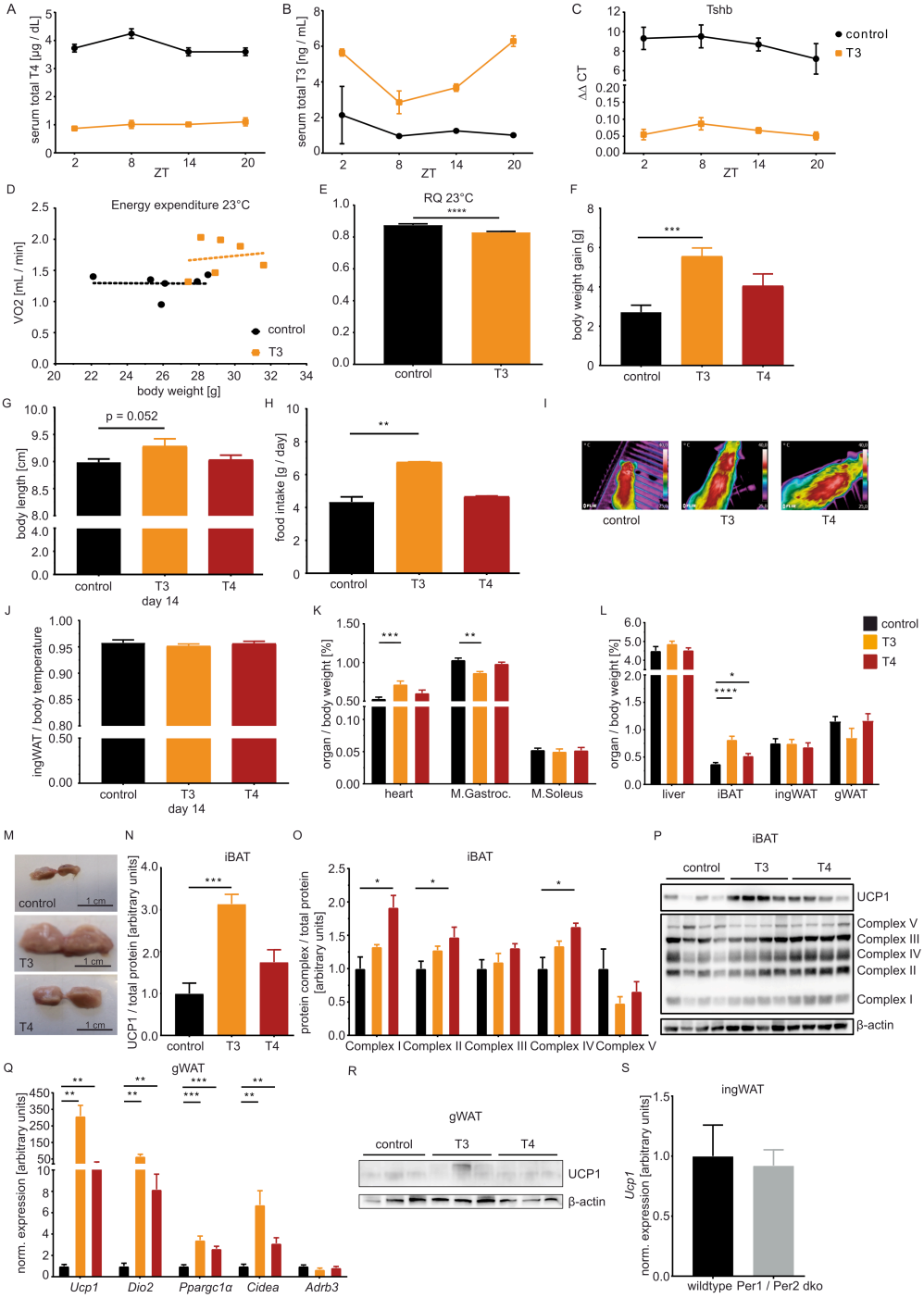

(A) Serum total T4, T3 (B) and pituitary *Tshb* (C) in control and T3-treated mice at 23°C over the course of 24 hours. n=3 per group and timepoint. (D) Energy expenditure in mice housed and treated for 10 days at 23°C. n=6. (E) Respiratory quotient (RQ) of control and T3-treated mice housed and treated for 10 days at 23°C. n=6. (F) Body weight gain over 14 days of treatment at 23°C. n=6-8. (G) Body length after 14 days of treatment at 23°C. n=6-8. (H) Food intake after 14 days of treatment at 23°C. n=2-4. (I) Infrared thermography after 14 days of treatment at 23°C. (J) ingWAT temperature measured by infrared thermography at the end of treatment normalized to body temperature. n=6-8. (K) Weights of heart, M. Gastrocnemius and M. Soleus after 14 days of treatment at 23°C, normalized to body weight at the time of sacrifice. n=6-8. (L) Weights of liver, iBAT, ingWAT and gWAT after 14 days of treatment at 23°C, normalized to body weight at the time of sacrifice. n=6-8. (M) Pictures of iBAT depots. (N) Quantification of UCP1 protein expression in iBAT at 23°C. n=4. (O+P) Protein expression of Complexes I - V of oxidative phosphorylation in iBAT at 23°C. n=4. (Q) Gene expression analysis of gWAT of control, T3- and T4-treated mice at 23°C. n=6-8. (R) UCP1 Western Blot in gWAT at 23°C. (S) *Ucp1* gene expression in ingWAT of WT and Per1/Per2 dko mice. n=3. Data are presented as mean ± SEM. *p<0.05, **p<0.01, ***p<0.001, ****p<0.0001

Figure S2, Related to Figure 2 and Figure 3

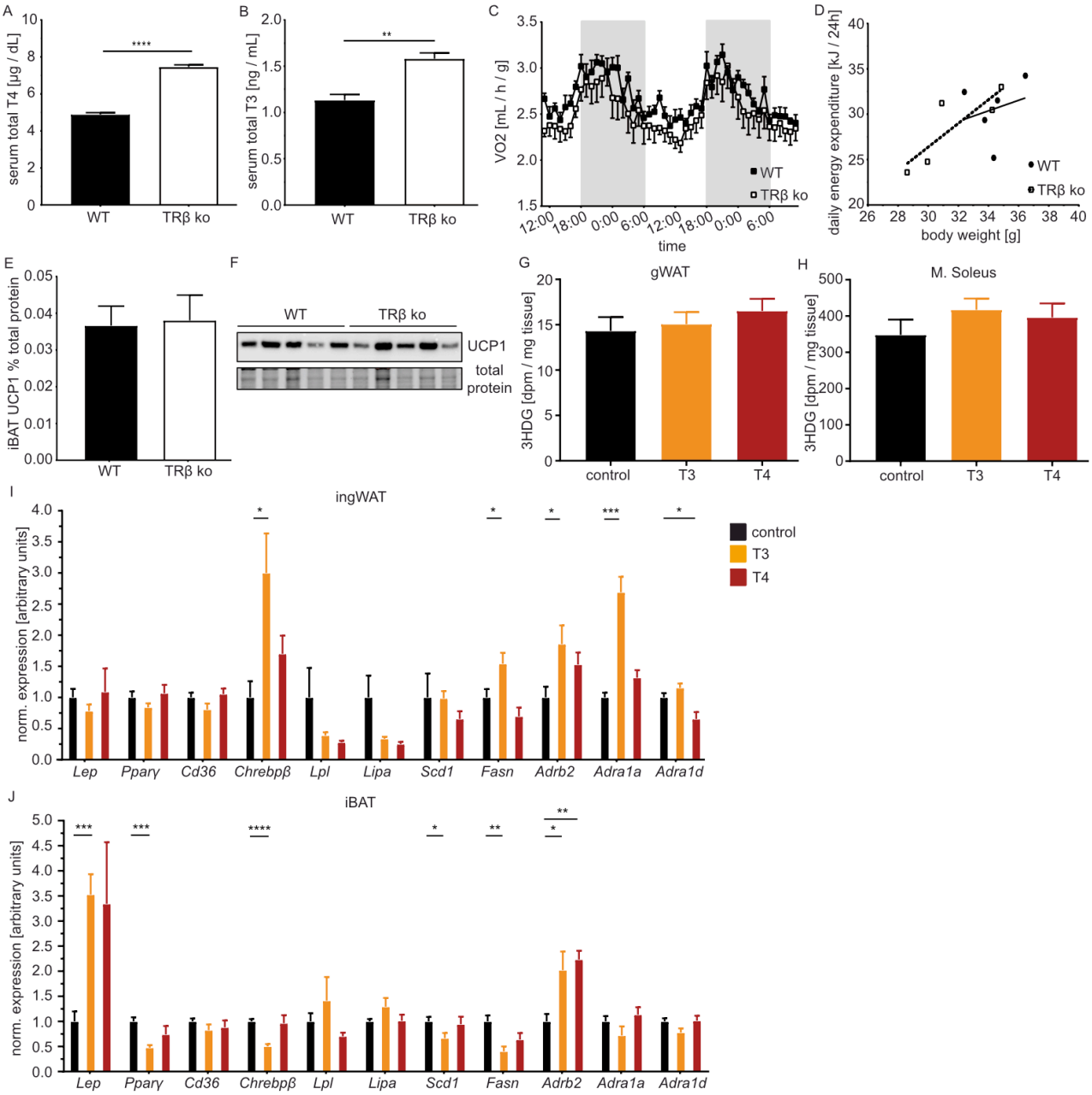

(A) Serum total T4 levels of WT and TRβ ko littermates. n=5. (B) Serum total T3 levels of WT and TRβ ko littermates. n=5. (C) Daily energy expenditure of WT and TRβ ko mice. Grey areas indicate nighttime. n=5. (D) Daily energy expenditure of WT and TRβ ko mice over body weight. n=5. (E) UCP1 protein expression in iBAT of WT and TRβ ko mice. n=5. (F) Representative Western Blot of UCP1 in iBAT of WT and TRβ ko mice. (G) ^{3}HDG uptake into gWAT of control, T3- and T4-treated mice. n=7-8. (H) ^{3}HDG uptake into M. Soleus of control, T3- and T4-treated mice. n=7-8. (I) Gene expression analysis in ingWAT and (J) iBAT of control, T3- and T4-treated mice at 23°C. n=6-8. Data are presented as mean ± SEM. *p<0.05, **p<0.01, ***p<0.001, ****p<0.0001

Figure S3, Related to Figure 4 and 5

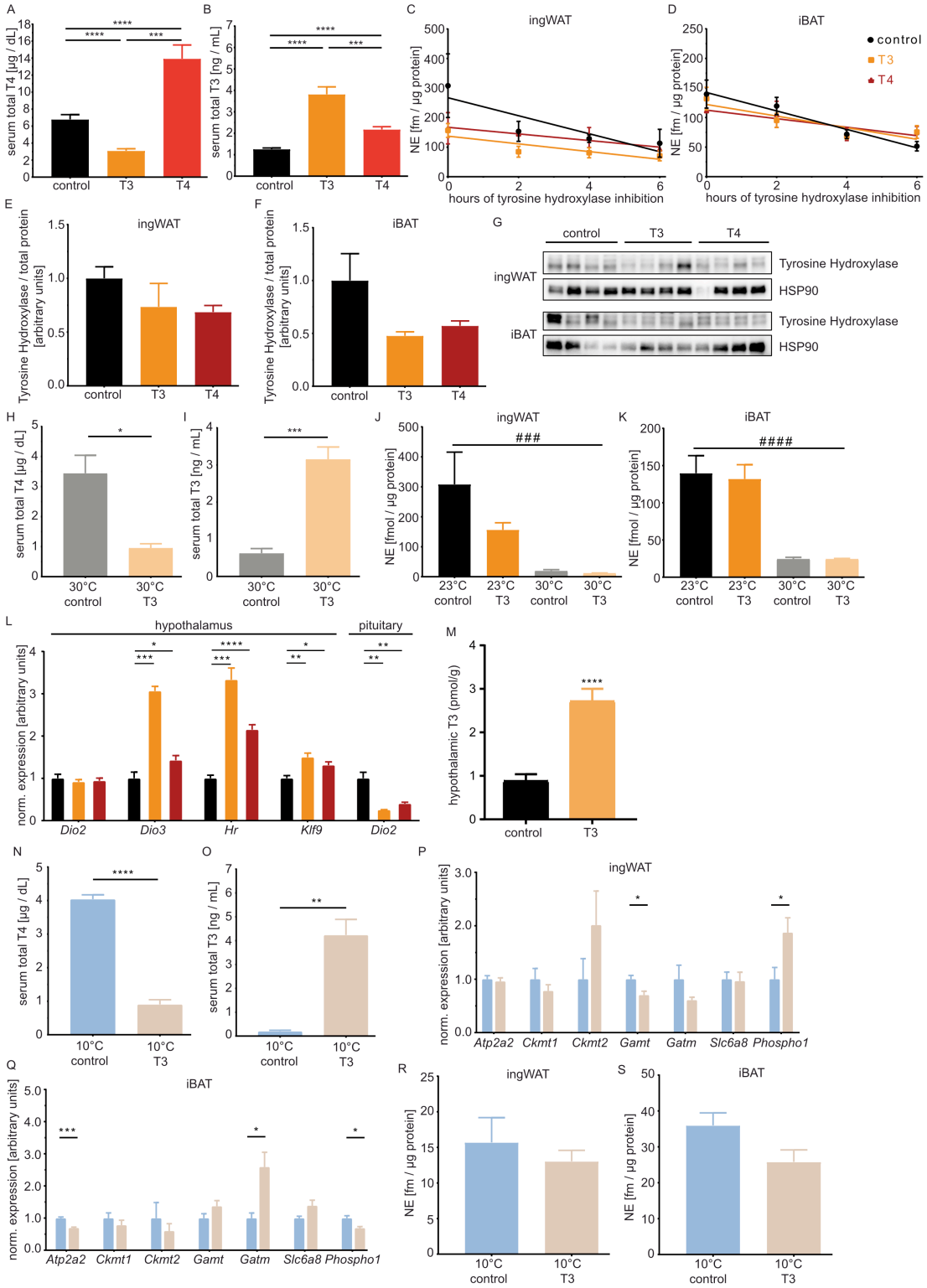

(A) Serum total T4 and T3 (B) levels after 14 days of treatment. n=16. (C) NE turnover in ingWAT and (D) iBAT. n=4 per group and timepoint. (E-G) Protein expression of tyrosine hydroxylase in ingWAT and iBAT. n=4. (H) Serum total T4 and T3 (I) after 14 days of treatment at 30°C. n=5. (J) NE content of ingWAT and (K) iBAT at 23°C or 30°C. n=4-5. (L) Gene expression in hypothalamus and pituitary at 23°C. n=6-8. (M) Hypothalamic T3 content in the T3 treated mice. n=15. (N) Serum total T4 and T3 (O) levels of mice at 10°C. n=6. (P) Gene expression in ingWAT and (Q) iBAT at 10°C. n=6. (R) NE levels in ingWAT and (S) iBAT at 10°C. n=6. Data are presented as mean ± SEM. *p<0.05, **p<0.01, ***p<0.001, $^{\#\#\#}p_{\text{ambient temperature}}<0.001$, $^{\#\#\#\#}p_{\text{ambient temperature}}<0.0001$

Figure S4, Related to Figure 6

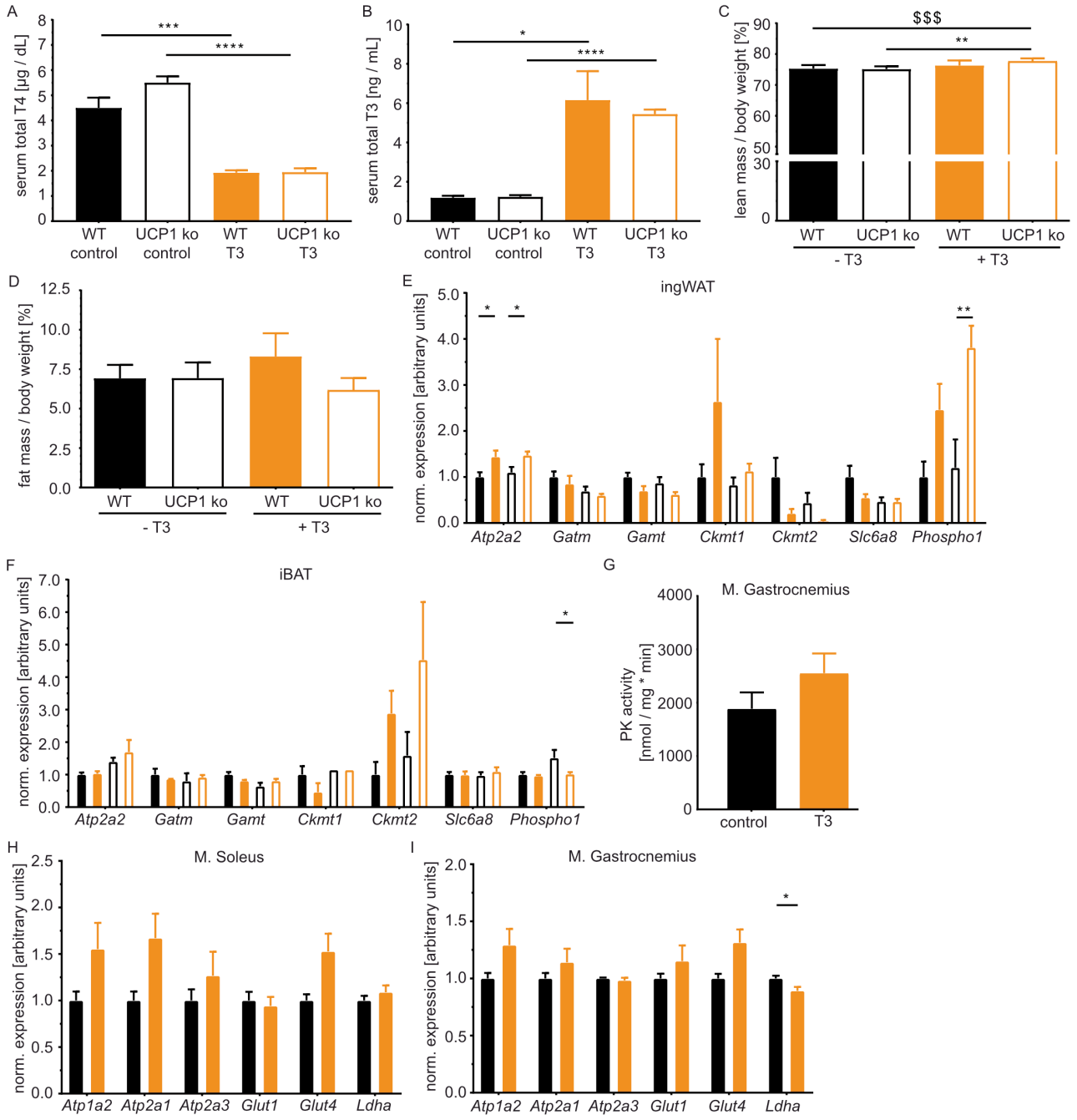

(A) Serum total T4 or T3 (B) levels of WT control, UCP1 ko control, T3-treated WT, and T3-treated UCP1 ko mice. n=5-8 . (C) Lean mass of WT and UCP1 ko mice before and after treatment with T3 for 14 days. n=5-6. (D) Fat mass of WT and UCP1 ko mice before and after treatment with T3 for 14 days. n=5-6. (E) Gene expression analysis of ingWAT and (F) iBAT of WT control, UCP1 ko control, T3-treated WT, and T3-treated UCP1 ko mice. n=5-8. (G) Pyruvate kinase activity in M. Gastrocnemius of control and T3-treated mice at 23°C. n=6-8. (H) Gene expression analysis of M. Soleus and (I) M. Gastrocnemius of control and T3-treated mice at 23°C. n=6-8. Data are presented as mean ± SEM. *p<0.05, **p<0.01, ***p<0.001, ****p<0.0001, $^{\$\$\$}p_{T3}$<0.001

Table S1: Statistical analysis of gene expression in ingWAT and iBAT of mice housed and treated with T3 at 23°C and 30°C, Related to Figure 4

	Thermoneutral + T3			Sidak	
ingWAT	interaction	ambient temp.	T3	23°C	30°C
Ucp1	****	****	****	****	ns
Dio2	***	****	****	****	ns
Ppargc1α	*	****	**	***	ns
Prdm16	ns	****	ns	*	ns
Adrb3	ns	ns	***	*	**

	Thermoneutral + T3			Sidak	
iBAT	interaction	ambient temp.	T3	23°C	30°C
Ucp1	***	*	ns	*	**
Dio2	**	***	*	***	ns
Ppargc1α	ns	ns	ns	ns	ns
Prdm16	**	***	**	***	ns
Adrb3	**	****	****	****	ns

Gene expression data were analysed using 2-way ANOVA with ambient temperature and treatment as independent factors. A Sidak correction was applied for the comparison between groups. ns= not significant, *p<0.05, **p<0.01, ***p<0.001, ****p<0.0001

Table S2: Statistical analysis of gene expression in ingWAT and iBAT of UCP1 KO and WT littermates treated with T3, Related to Figure 6

	UCP1 KO + T3			**Sidak**	
ingWAT	interaction	genotype	T3	WT	UCP1 KO
Dio2	ns	**	**	*	ns
Ppargc1α	ns	ns	ns	ns	ns
Prdm16	ns	ns	ns	ns	ns
Tmem26	ns	ns	ns	ns	ns
Cidea	ns	**	**	ns	*
Adrb3	ns	ns	ns	ns	ns
Atp2a2	ns	ns	***	*	*
Gatm	ns	*	ns	ns	ns
Gamt	ns	**	ns	ns	ns
Ckmt1	ns	ns	ns	ns	ns
Ckmt2	ns	ns	*	ns	ns
Slc6a8	ns	ns	ns	ns	ns
Phospho 1	ns	ns	**	ns	**

	UCP1 KO + T3			Sidak	
iBAT	interaction	genotype	T3	WT	UCP1 KO
Dio2	ns	*	***	ns	**
Ppargc1α	ns	ns	***	ns	***
Adrb3	ns	ns	**	*	*
Atp2a2	ns	*	ns	ns	ns
Gatm	ns	ns	ns	ns	ns
Gamt	*	*	ns	ns	ns
Ckmt1	ns	ns	ns	ns	ns
Ckmt2	ns	ns	ns	ns	ns
Slc6a8	ns	ns	ns	ns	ns
Phospho1	ns	*	ns	ns	*

Gene expression data were analysed using 2-way ANOVA with genotype and treatment as independent factors. A Sidak correction was applied for the comparison between groups. ns= not significant, *p<0.05, **p<0.01, ***p<0.001, ****p<0.0001

Table S3: Primer Sequences, Related to STAR Methods

REAGENT or RESOURCE			SOURCE	IDENTIFIER
Oligonucleotides				
Adrb3	for	AGA AAC GGC TCT CTG GCT TTG	IDT, Inc, Germany	N/A
Adrb3	rev	TGG TTA TGG TCT GTA GTC TCG G	IDT, Inc, Germany	N/A
Atp1a2	for	CCA CCA CTG CGG AAA ATG G	IDT, Inc, Germany	N/A
Atp1a2	rev	GCC CTT AGA CAG ATC CAC TTG G	IDT, Inc, Germany	N/A
Atp2a1	for	TGT TTG TCC TAT TTC GGG GTG	IDT, Inc, Germany	N/A
Atp2a1	rev	AAT CCG CAC AAG CAG GTC TTC	IDT, Inc, Germany	N/A
Atp2a2	for	TCC GCT ACC TCA TCT CAT CC	IDT, Inc, Germany	N/A
Atp2a2	rev	CAG GTC TGG AGG ATT GAA CC	IDT, Inc, Germany	N/A
Atp2a3	for	CGT CGC TTC TCG GTG ACA G	IDT, Inc, Germany	N/A
Atp2a3	rev	AAG AGG TCC TCA AAC TGC TCC	IDT, Inc, Germany	N/A
Cd36	for	ATG GGC TGT GAT CGG AAC TG	IDT, Inc, Germany	N/A
Cd36	rev	GTC TTC CCA ATA AGC ATG TCT CC	IDT, Inc, Germany	N/A
Chrebpβ	for	TCT GCA GAT CGC GTG GAG	IDT, Inc, Germany	N/A
Chrebpβ	rev	CTT GTC CCG GCA TAG CAA C	IDT, Inc, Germany	N/A
Cidea	for	TGA CAT TCA TGG GAT TGC AGA	IDT, Inc, Germany	N/A
Cidea	rev	GGC CAG TTG TGA TGA CTA AGA	IDT, Inc, Germany	N/A
Ckmt1	for	TGT CTT CAA GAG TCA GAA CTG GC	IDT, Inc, Germany	N/A
Ckmt1	rev	AGC ATC CAC CAC AAC ACG TT	IDT, Inc, Germany	N/A
Ckmt2	for	ACA CCC AGT GGC TAT ACC CTG	IDT, Inc, Germany	N/A
Ckmt2	rev	CCG TAG GAT GCT TCA TCA CCC	IDT, Inc, Germany	N/A
Dio2	for	ATG GGA CTC CTC AGC GTA GAC	IDT, Inc, Germany	N/A
Dio2	rev	ACT CTC CGC GAG TGG ACT T	IDT, Inc, Germany	N/A
Fasn	for	GGA GGT GGT GAT AGC CGG TAT	IDT, Inc, Germany	N/A
Fasn	rev	TGG GTA ATC CAT AGA GCC CAG	IDT, Inc, Germany	N/A
Gamt	for	CAC GCA CCT GCA AAT CCT G	IDT, Inc, Germany	N/A
Gamt	rev	TAC CGA AGC CCA CTT CCA AGA	IDT, Inc, Germany	N/A
Gatm	for	GCT TCC TCC CGA AAT TCC TGT	IDT, Inc, Germany	N/A
Gatm	rev	CCT CTA AAG GGT CCC ATT CGT	IDT, Inc, Germany	N/A
Glut1	for	TCA AAC ATG GAA CCA CCG CTA	IDT, Inc, Germany	N/A
Glut1	rev	AAG AGG CCG ACA GAG AAG GAA	IDT, Inc, Germany	N/A
Glut4	for	GTG ACT GGA ACA CTG GTC CTA	IDT, Inc, Germany	N/A
Glut4	rev	CCA GCC ACG TTG CAT TGT AG	IDT, Inc, Germany	N/A
Gpd2	for	GAA GGG GAC TAT TCT TGT GGG T	IDT, Inc, Germany	N/A
Gpd2	rev	GGA TGT CAA ATT CGG GTG TGT	IDT, Inc, Germany	N/A
Ldha	for	CAT TGT CAA GTA CAG TCC ACA CT	IDT, Inc, Germany	N/A
Ldha	rev	TTC CAA TTA CTC GGT TTT TGG GA	IDT, Inc, Germany	N/A
Lep	for	GAG ACC CCT GTG TCG GTT C	IDT, Inc, Germany	N/A
Lep	rev	CTG CGT GTG TGA AAT GTC ATT G	IDT, Inc, Germany	N/A
Lipa	for	AGC GAC GAC TTG GTG TTC C	IDT, Inc, Germany	N/A
Lipa	rev	GCT GAG CAA GAC TCC ACC G	IDT, Inc, Germany	N/A
Lpl	for	GGT TGC GCG TAG AGA GGA TG	IDT, Inc, Germany	N/A

REAGENT or RESOURCE			SOURCE	IDENTIFIER
Oligonucleotides				
Lpl	rev	CTC ACG CTC TGA CAT GCC TTC	IDT, Inc, Germany	N/A
Phospho1	for	ATG AGC GGG TGT TTT CCA G	IDT, Inc, Germany	N/A
Phospho1	rev	ATC GAA GTC GAA GGT GAG GAG	IDT, Inc, Germany	N/A
Pparδ	for	TCC ATC GTC AAC AAA GAC GGG	IDT, Inc, Germany	N/A
Pparδ	rev	ACT TGG GCT CAA TGA TGT CAC	IDT, Inc, Germany	N/A
Pparγ	for	TCG CTG ATG CAC TGC CTA TG	IDT, Inc, Germany	N/A
Pparγ	rev	GAG AGG TCC ACA GAG CTG ATT	IDT, Inc, Germany	N/A
Ppargc1α - total	for	TGA TGT GAA TGA CTT GGA TAC A	IDT, Inc, Germany	N/A
Ppargc1α - total	ref	GCT CAT TGT TGT ACT GGT TGG A	IDT, Inc, Germany	N/A
Ppia	for	GCA GTA CAG CCC CAA AAT GG	IDT, Inc, Germany	N/A
Ppia	rev	AAC AAA GTC TGG CCT GTA TCC AA	IDT, Inc, Germany	N/A
Prdm16	for	CCC CAC ATT CCG CTG TGA T	IDT, Inc, Germany	N/A
Prdm16	rev	CTC GCA ATC CTT GCA CTC A	IDT, Inc, Germany	N/A
Rplp0	for	TCG GGT CCT AGA CCA GTG TTC	IDT, Inc, Germany	N/A
Rplp0	rev	AGA TTC GGG ATA TGC TGT TGG C	IDT, Inc, Germany	N/A
Ryr1	for	CAG TTT TTG CGG ACG GAT GAT	IDT, Inc, Germany	N/A
Ryr1	rev	CAC CGG CCT CCA CAG TAT TG	IDT, Inc, Germany	N/A
Scd1	for	TTC TTG CGA TAC ACT CTG GTG C	IDT, Inc, Germany	N/A
Scd1	rev	CGG GAT TGA ATG TTC TTG TCG T	IDT, Inc, Germany	N/A
Slc6a8	for	GTC TGG TGA CGA GAA GAA GGG	IDT, Inc, Germany	N/A
Slc6a8	rev	CCA CGC ACG ACA TGA TGA AGT	IDT, Inc, Germany	N/A
Sln	for	GAGGTGGAGAGACTGAGGTCCTTGG	IDT, Inc, Germany	N/A
Sln	rev	GAAGCTCGGGGCACACAGCAG	IDT, Inc, Germany	N/A
Tfam	for	GGA ATG TGG AGC GTG CTA AAA	IDT, Inc, Germany	N/A
Tfam	rev	TGC TGG AAA AAC ACT TCG CAA TA	IDT, Inc, Germany	N/A
Tfam	for	GGA ATG TGG AGC GTG CTA AAA	IDT, Inc, Germany	N/A
Tfam	rev	ACA AGA CTG ATA GAC GAG GGG	IDT, Inc, Germany	N/A
Tmem26	for	TTC CTG TTG CAT TCC CTG GTC	IDT, Inc, Germany	N/A
Tmem26	rev	GCC GGA GAA AGC CAT TTG T	IDT, Inc, Germany	N/A
Ucp1	for	ACT CAG GAT TGG CCT CTA CG	IDT, Inc, Germany	N/A
Ucp1	rev	CCA CAC CTC CAG TCA TTA AGC	IDT, Inc, Germany	N/A
Ucp3	for	GAG ATG GTG ACC TAC GAC ATC A	IDT, Inc, Germany	N/A
Ucp3	rev	GCG TTC ATG TAT CGG GTC TTT A	IDT, Inc, Germany	N/A